1

Fundamentals of Conjugated Polymer Nanostructures

Thanh-Hai Le[1] *and Hyeonseok Yoon*[1,2]

[1] *Chonnam National University, Graduate School, Department of Polymer Engineering, 77 Yongbong-ro, Gwangju 61186, South Korea*
[2] *Chonnam National University, School of Polymer Science and Engineering, 77 Yongbong-ro, Gwangju 61186, South Korea*

1.1 Introduction

Earlier research on the design and development of materials related to conjugated polymers has attracted renewed interest, which has contributed to the materials being accepted as robust alternatives to their inorganic counterparts, therefore leading to large and substantial practical research efforts. Since the time when polyacetylene was discovered in 1977 by Hideki Shirakawa, Alan Heeger, and Alan MacDiarmid, many kinds of conjugated polymers have been developed, such as polypyrrole (PPy), polyaniline (PANI), polythiophene (PT), poly(*p*-phenylene vinylene) (PPV), and their derivatives [1]. Conjugated polymers contain a carbon backbone, which holds interchanging single (σ) and double (π) bonds that allow electrons to be delocalized, and thus contribute towards various electronic, electrical, electrochemical, and optical characteristics. Owing to the π-conjugated system coupled with the inherent characteristics of polymers, conjugated polymers have competitive properties over those of their inorganic counterparts, such as mild synthetic conditions, chemical diversity, structural flexibility, tunable electrical/optical properties, anticorrosion, and lightweight [2, 3]. Note also that, by converting bulk conjugated polymers into nanostructures, the resulting nano-dimensionality features can lead to beneficial properties, such as quantized energy level, enlarged surface area, more efficient and rapid doping/dedoping, and enhanced crystallinity [4–7]. Conjugated polymers have been hybridized with other functional materials to overcome their limitations in terms of conductivity, stability, and solubility. These materials have been successfully utilized in a wide range of optoelectronic [8–12], energy conversion [13, 14], energy storage [15, 16], photocatalytic [4, 17], and biomedical applications [5, 18].

This chapter will present the fundamentals of conjugated polymer and their nanostructures, and focus on electronic, electrical, optical, and electrochemical properties. These properties depend on the dopants, doping level, and inherent

Conjugated Polymer Nanostructures for Energy Conversion and Storage Applications,
First Edition. Edited by Srabanti Ghosh.

properties of conjugated systems such as chain conformation, aggregation state, shape, and size of the nanomaterials. Better understanding of these properties and charge transport mechanisms will contribute to extending the use of conjugated polymers over a wide range of applications, from optoelectronic to medical applications, as well as in energy conversion/storage devices and systems.

1.2 Electronic and Electrical Properties

1.2.1 Conductive Mechanism

1.2.1.1 Inherent Molecular Structure

In general, energy band theory has been used to clarify the key differences between semiconductors, conductors, and insulators. The band gap is identified as being the energy difference between the lowest unoccupied molecular orbital (LUMO) of the conduction band and the highest occupied molecular orbital (HOMO) of the valence band in a material. In conductor materials, the conduction band overlaps the valence band, such that electrons are able to move freely and disseminate between the two bands. In contrast, semiconductor materials can conduct electricity under some excitation conditions because of their small band gap. When the band gap becomes too large for electrons to cross (no electricity is conducted), the material is known as an insulator. Energy band theory fails to explain why conjugated polymers, which are organic materials, can conduct electricity. The charge transport mechanisms of conjugated polymer at the molecular level have been investigated from both theoretical and experimental evidences by many research groups [19, 20]. The most commonly accepted mechanism based on the high electrical conductivity and simple chemical structure of polyacetylene is represented in Figure 1.1. In general, the existence of interchanging single and double bonds through the polymer backbone is an inherent property of conjugated polymers. These single and double bonds contain a localized σ-bond, which is known to allow formation of a strong chemical bond. Moreover, it is recognized that each double bond also holds a **delocalized π-bond**, which is however weaker compared with the σ-bond [21, 22]. Here, the overlap between p_z-orbitals in the chain of conjugated π-bonds allows the π-electrons to freely move across the carbon backbone. As a result, the conjugated π-bonds can

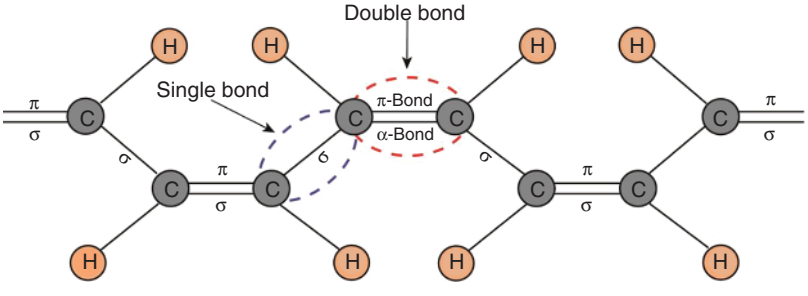

Figure 1.1 Scheme describing the conjugated π-system in *cis*-polyacetylene.

conduct electricity. However, it is believed that conjugated π-bonds cannot make conjugated polymers become high-conductivity materials owing to a distinct disorder in the polymer matrix. Structural and morphological disorders hinder delocalization of π-electrons, thus delaying charge transport along the polymer chain [23–25]. Consequently, the metallic charge conduction of a pristine conjugated polymer is fairly weak. A discovery by Hideki Shirakawa, Alan Heeger, and Alan MacDiarmid on electrically conductive polyacetylene modified the ways that physicists and chemists think about conductance in polymeric materials. The work involved using an external exciting factor called "doping," whereby a halogen dopant removes an electron from a delocalized π-bonding of polyacetylene and creates a hole. In turn, an electron of an adjacent double bond is delocalized and couples with the hole, which generates a new hole, therefore, allowing very high conductivities of up to 10^5 S/cm. Since this pioneering work was published, many theories have been proposed to explain the conductivity mechanism of conjugated polymers. Some formations of local excitations, such as polarons, bipolarons, and solitons, have been considered as charge carriers [20, 26, 27].

1.2.1.2 Doping and Band Structure Evolution

The conductivity of pristine conjugated polymers is in the range of 10^{-6}–10^{-10} S/cm, which is at the boundary between an insulator and a semiconductor (Figure 1.2). However, their conductivities can be tuned through the process of doping [28]. The structural and morphological disorder can be reduced when conjugated systems are doped. Doping induces the formation of charge carries such as solitons, polarons, and bipolarons, which reduce lattice distortion [29]. As a result, doping has contributed towards the creation of novel conjugated polymers, whereby the conductivity of the pristine system can be upgraded to semiconducting or even metallic levels. For example, polyacetylene doped with iodine achieved a high conductivity of approximately 10^4 S/cm, as reported by Tsukamoto et al. [30, 31], which is as high as the conductivity of lead at room temperature (4.8×10^4 S/cm). Through the achievement of high conductivity, conjugated polymers have gradually become more useful as candidate materials for various practical applications.

Doping in semiconductors is the process of introducing impurities into the crystal lattice of the material to modulate its conductivity. The number of valence electrons of the impurity, namely, the dopant, defines the type of doping and

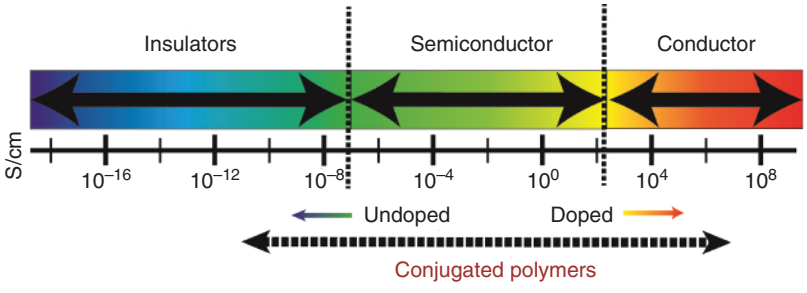

Figure 1.2 Conductivity range of conjugated polymers based on doped/undoped states.

conductivity of semiconductor materials. For example, a silicon atom has four electrons in its outer shell. When a phosphorus atom (five valence electrons) or boron atom (three valence electrons) replaces a silicon atom, it will form negative (a free electron, p-type doped) or positive sites (a hole, n-type doped), respectively, on the crystal lattice of silicon. These sites play the role of charge carriers, and increase the conductivity of the silicon crystal by up to 10^6 S cm^{-1}. Because of the π-conjugated system, it is acknowledged that the doping mechanism of polymers is completely different from that of conventional semiconductors [28]. From the electron transfer aspect, the doping in conjugated polymers is a partial redox process, which generates delocalized charges on the polymer backbone [30]. The dopant plays the role of supplying additional electrons to the conjugated polymer or removing electrons from the polymer chain. Its mechanism is related to the process of adding electrons to the lowest available energy state of the conduction band (reduction) or removing electrons from the highest available energy state of the valence band (oxidation). The reduction or oxidation process is known to construct charge carriers, which are commonly described in various forms such as polarons, bipolarons, or solitons, in conjugated polymers. Typically, conjugated polymers exist in the form of non-degenerate or degenerate systems based on their ground state structure. The nondegenerate ground-state polymers have two different electronic structures with different energies, such as polyacetylene [32, 33], whereas degenerate ground-state polymers have identical electronic structures and energies, such as poly(tetraphenylquinodimethans) (PTPhQ), polyparaphenylene, polythiophene, PANI, and PPy [32, 34]. Both polarons and bipolarons have been detected as the charge carriers in non-degenerate systems, while solitons play the role of charge carriers in degenerate systems [19, 29, 34, 35]. Consequently, the flow/delocalization of charge carriers along the skeleton backbone allows the polymer to be conductive. The reduction and oxidation processes of conjugated polymers are related to the concept of p-type and n-type doping in organic semiconductors, respectively [11, 26]. From the perspective of physicists and chemists, n-type doping of conjugated polymers is known as the transfer of electrons from the HOMO of the dopant species to the LUMO of the polymer, which results in augmented electron density. On the other hand, in p-type doping, an electron from the HOMO of the polymer moves to the LUMO of the dopant species, therefore creating a hole within the polymer chain. Henceforth, the amount of incorporated dopant ions to the unit monomers of conjugated polymers is defined as the doping level. Controlling the doping level can tune the mobility and density of the charge carriers and thus the conductivity of conjugated polymers [36–38].

In general, a conjugated polymer is capable of sustaining/encountering p-type doping or n-type doping through an oxidation or reduction step to be conductive. The oxidation/reduction processes will lead to the formation of either negative or positive polarons/bipolarons, as presented in Figure 1.3. The positively charged forms provide p-type doping, while negatively charged forms provide n-type doping. The delocalization of these polarons/bipolarons along the polymer backbone leads to enhanced electronic conductivity. As has been reported, the negative polaron/bipolaron ratio in n-doping is not stable in comparison with the positive

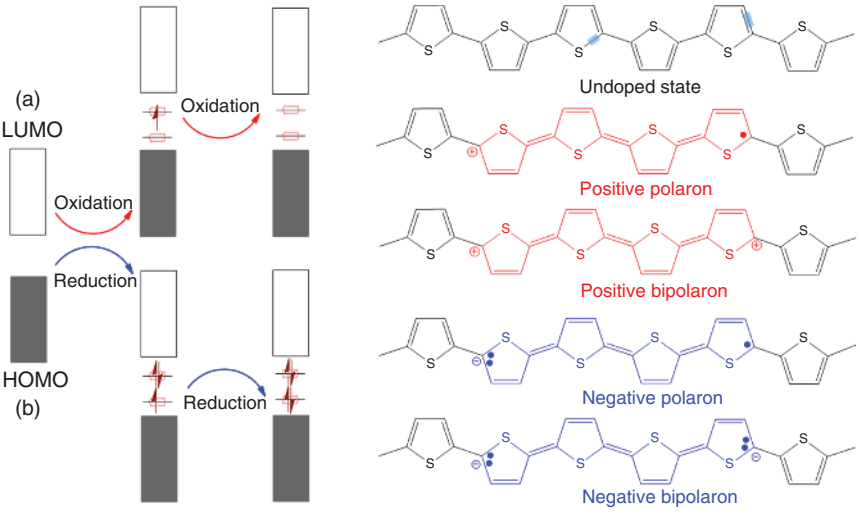

Figure 1.3 Electronic band and chemical structures of polythiophene (PT) with (a) p-type doping and (b) n-type doping. Source: Le et al. [26]. Licensed under CC BY 4.0.

forms, making the p-doping option more common in fundamental research as well as in practical applications. For example, p-doping of nondegenerate ground-state PPy has been reported as capable of creating different electronic energy band structures as the doping level increases. Pristine or undoped PPy has a wide band gap of approximately 3.16 eV and hence is considered to be an insulator (Figure 1.4a). Once oxidation starts occurring owing to halogen doping, π-electrons are removed from the HOMO of pristine PPy, which involves the transformation of a benzoid-like to a quinoid structure, forming radical cations, namely, positive polarons [20, 39]. This takes place along with the appearance of two new symmetric electronic states within the band gap, which reduces the band gap from 3.16 to 2.26 eV (Figure 1.4b). Upon increasing the oxidation level, a second electron is transferred from the HOMO of PPy to the LUMO of the dopant, forming a di-cation, which is a positive bipolaron (Figure 1.4c). In other words, PPy has higher quinoid features in the bipolarons as compared with polarons. Further oxidation of PPy will cause an overlap of neighboring bipolarons to form new contracted bipolaronic bands, as presented in Figure 1.4d. Thus, p-doping induces new electronic states or optical transitions in the energy band structure of PPy, which can be observed as longer wavelength absorptions.

In comparing degenerate with nondegenerate ground-state polymers, the degenerate ground-state polymer has a simpler model, known as a *trans*-polyacetylene. When polyacetylene encompasses an uneven number of carbon atoms in the polymer chain, the interchange of single and double bonds will produce a conjugated system with two similar electronic structures (A and B phases) and identical energies (Figure 1.5a). The neutral state of the polyacetylene contains an unpaired electron between the two structures, which is also known as a neutral soliton (Figure 1.5d). While delocalizing along the polymer backbone, if a neutral soliton meets another,

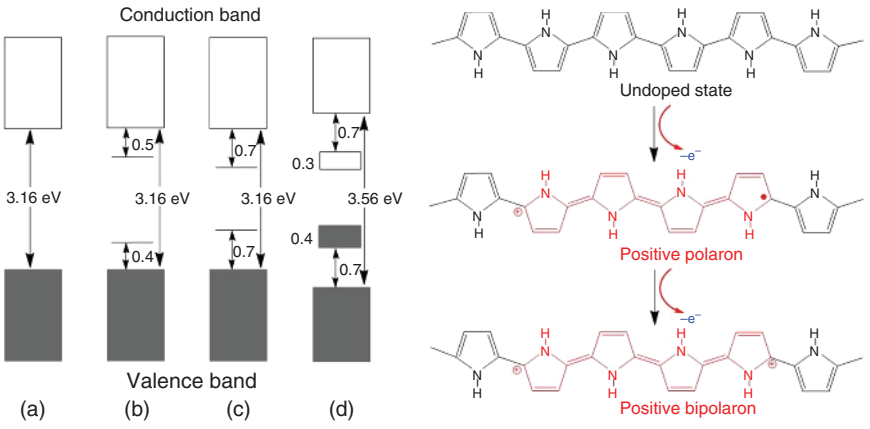

Figure 1.4 Electronic bands and chemical structures illustrating (a) undoped; (b) polaron; (c) bipolaron; and (d) fully doped states of polypyrrole (PPy). Source: Le et al. [26]. Licensed under CC BY 4.0.

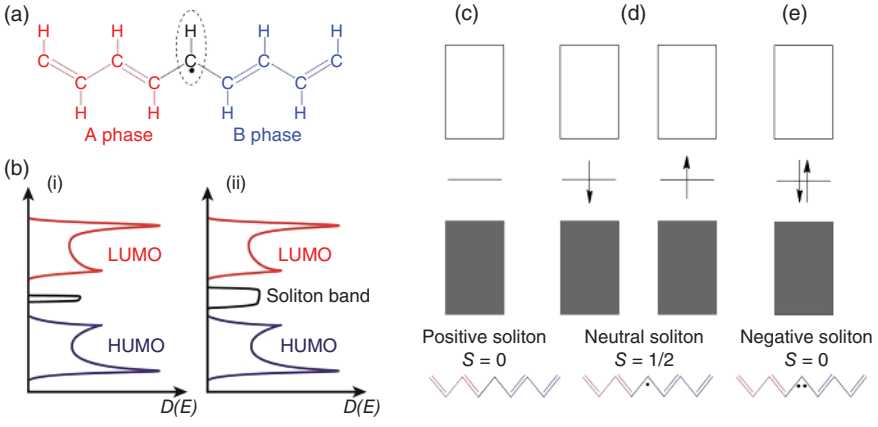

Figure 1.5 (a) Schematic illustration of the geometric structure of a neutral soliton on a trans-polyacetylene chain; (b) a soliton band with light doping (i) and heavy doping (ii); The band structure of trans-polyacetylene containing (c) a positively charged soliton, (d) a neutral soliton, and (e) a negatively charged soliton. Source: Le et al. [26]. Licensed under CC BY 4.0

they will combine and generate a double bond. When *trans*-polyacetylenes undergo an oxidation or reduction process by a dopant species, a neutral soliton can either receive or donate an electron, which results in the generation of positive or negative spin-less solitons ($S = 0$) (Figure 1.5c,e). In the transport along the polymer chain, the charged soliton can overlap with others, which leads to the formation of a soliton band-like structure [26, 40, 41]. This band can be expanded by increasing the oxidation/reduction level and lies between the HOMO and LUMO of *trans*-polyacetylene (Figure 1.5b). When the structure becomes a nondegenerate ground-state system such as *cis*-polyacetylene, the solitons become unstable in this polymer and tend to transform to polarons/bipolarons.

Overall, polarons, bipolarons, and solitons play the role of charge carriers and enable electrical conductivity in nondegenerate and degenerate ground-state conjugated polymers and their nanostructures [20]. There are major external factors that impact conjugated polymer conductivity, e.g. temperature, as well as the degree of doping and chain orientation. Additional factors will be discussed in Sections 1.3.2 and 1.3.3.

1.2.2 Charge Carrier Transport Models

In principle, the electrical properties of conjugated polymers have a strong dependence on the presence of disorder in the material, including main and end chains, external coupling, voids, entangled chains, and doping deficiencies/blemishes. Initially, it was difficult to understand disordered materials, so the issue was avoided, or the materials were forced into ordered systems. Since Anderson presented the basic concept of localization in 1958, localized electrons could be used to explain the charge transport properties observed in homogeneously disordered materials. It is known that within a perfect crystal with periodic potentials, the wave functions will form Bloch waves, which can delocalize in a mean free path (l) throughout the structure of materials (electrons tend to hop from site to site, which leads to generating a band). On the other hand, the degree of disorder can change the wave function. For example, within disordered systems, structural defects and impurities cause significant electronic wave function scattering, which can result in localization. If the material has strong disorder, the overlap of the wave function may decline rapidly and thus the system exhibits higher insulator behavior. The localized wave function (Ψ) can be expressed as

$$\Psi(r) \infty \exp\left(-\frac{r - r_0}{\xi}\right) \tag{1.1}$$

where r is the position and ξ is the localization length of the state of an atom. In later years, Mott recognized that electrons at the center of the band can be delocalized, whereas electrons at the band tail tend to localize owing to the contribution of electrons from localized orbitals in deep potential fluctuations [42, 43]. Here, the critical energy (E_c) was proposed in terms of the "mobility edge" to describe the transition point between the extended and localized states of electrons, which appeared as a band inside the band gap (Figure 1.6). The locations of the Fermi level (E_F) and E_c determine the conductivity in different materials. When the position of E_F is in the region of the localized states, the conductivity of the material vanishes, therefore exhibiting non-metallic behavior, despite there being a limited density of states at the Fermi level. Conversely, if E_F lies in the region of the extended states, as shown in Figure 1.6c, the material exhibits metallic behavior at low temperature and possesses a finite DC conductivity. Therefore, the mobility edge specifying the metal–insulator transitions and the DC conductivity can be found from the Drude or Boltzmann theory, where the DC conductivity (σ) of weak disordered materials is described by

$$\sigma = \frac{ne^2\tau}{m} \tag{1.2}$$

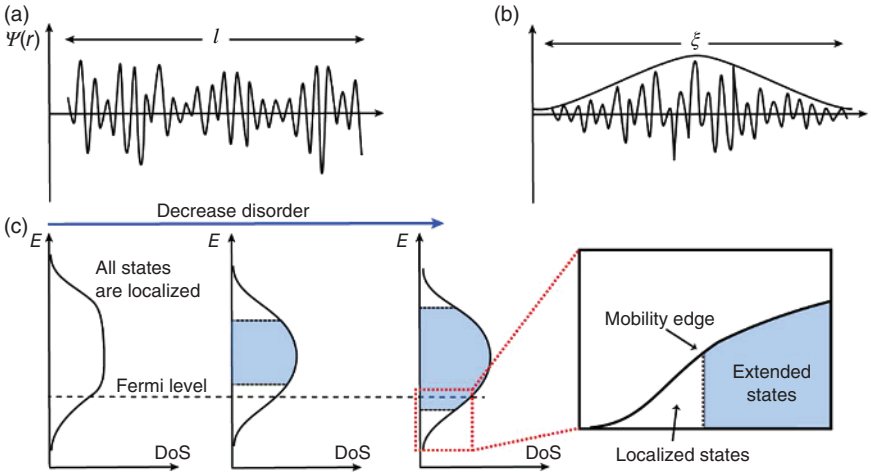

Figure 1.6 Anderson metal–insulator transition in single-band model. (a) Typical wave function of localization state with localization length, (b) extended block wave function with the mean free path, and (c) mobility edge in a disordered system.

where e is the electronic charge, $\tau = \frac{l}{v_F}$ is the relaxation time, and m and n are the effective mass and density of the carrier, respectively [43–46]. In weak disordered systems, the Fermi wavelength (k_F) is much shorter than the mean free path, and thus $k_F l \gg 1$ in this system.

$$k_F l = \frac{\left[h(3\pi^2)^{\frac{2}{3}}\right]}{e^2 \rho n^{1/3}} \tag{1.3}$$

In (1.3), ρ is the resistivity. The theory of Anderson localization does not fully describe the electrical properties/metallic state of highly doped conjugated polymers. Therefore, Epstein et al. [47] pointed out the delocalization of charges in conjugated polymers based on the study of an inhomogeneous disordered model, which is related to 3D metallic crystalline domains (such as rod-like [weakly metallic system], expanded "mesoscopic" coil-like, expanded coil-like, and weakly linked fibers) affected by a disordered quasi-1D medium [48, 49]. According to experimental data, the model agrees well with the frequency-dependent dielectric constant of doped PANI and PPy [47–49]. Moreover, the classic Mott's variable range hopping model can be used to explain the charge transport based on the hopping of states, charge carriers in disordered systems, or energy-limited tunneling between domains near the Fermi energy [50, 51]. For highly doped polymers, l is approximately 10 Å, charge-carrier density is of the order of 10^{21} cm^{-3}, and $k_F l \approx 1$–10 at room temperature. The metallic states of various conjugated polymers have been reported, and Table 1.1 summarizes these.

The concentration of the dopant, doping time, and distinction of the polymer that affect the conductivity of conjugated polymers implies a complicated internal mechanism. Many authors from the research community have made an effort to improve the conductivity of conjugated polymers by using different types of

Table 1.1 Maximum metallic states observed in doped conjugated polymers.

Conjugated polymer	Repeat unit	Chain orientation	Conductivity (S/cm)
Polyacetylene	C_2H_2	High	10^4–10^5
PPV	C_6H_4-C_2H_2	High	10^4
PPy	C_5H_2N	Low	400
PANI	C_6H_4-NH	Low	400
Poly(3-methylthiophene)	C_5H_2S-CH_3	Low	400
PEDOT	$C_7H_4O_2S$	Low	300

Source: Le et al. [26]. Licensed under CC BY 4.0.

dopants. According to their chemical nature, dopants can be classified into three groups, including inorganic (i.e. halogens, lithium, $MgCl_2$, $HClO_4$), organic (i.e. quaternary ammonium salts, acid acetic, hydroquinone-2), and large polymeric (i.e. polystyrene sulfonic acid, poly(2-acrylamido-2-methyl-propane sulfonic acid, polyvinyl phosphate) dopants). Table 1.2 shows the conductivities of conjugated polymers using various dopants, as reported in the literature to date. It is acknowledged that the chemical nature of the dopant species can affect both the structure and conductivity of conjugated polymers. Conjugated polymers can achieve very high conductivity with various small inorganic species as compared with organic and polymeric species. However, they have poor environmental stability owing to the high de-inserting, exchanging, and hydrophilic properties of small inorganic dopants. Large organic and polymeric dopants, in contrast, can improve the solubility, processability, and stability of conjugated polymers in various organic and aqueous phases by choosing the appropriate species. Because of their large chemical structure, large organic and polymeric molecules can limit the charge mobility in the polymer, affect the density of the polymer, and theretofore change the physical properties and surface topography of doped polymers. However, the strong adhesion of these dopants on conjugated polymers prevents the use of the polymer in many applications based on the insertion/de-insertion mechanism needed for supercapacitors, batteries, and electrochromic devices [52].

In general, the conductivity of conjugated polymers dramatically increases with an increase in the doping level. Tsukamoto et al. demonstrated the relationship between dopant ions and the electrical conductivity of conjugated polymers based on a study of I_2 doped stretched polyacetylene [30, 31]. In the initial observation, the gradually increasing conductivity of polyacetylene by I_2 doping implied the generation of highly ordered stacking structures, which are responsible for high conductivity rather than the primary structure of the polymer. After eight hours of doping, the conductivity saturated, which indicated the slow diffusion of the I_2 ions into the matrix of the polymer [30, 31]. In other words, the conductivity of conjugated polymers is proportional to the doping level and becomes saturated at high levels of dopant ions (fully doped level). Along with doping, de-doping is the process of reproducing the pristine conjugated polymer without degradation of the

Table 1.2 Typical examples of dopants for conjugated polymers and corresponding conductivities.

Conjugated polymer	Dopant	Chemical source	Doping method	Conductivity (S/cm)
Trans-polyacetylene	Na^+	$(C_{10}H_8)Na$	Solution doping	80
Poly(*p*-phenylene)	AsF_5	AsF_5	Vapor phase doping	1.5×10^4
Poly(*p*-phenylene vinylene)	CH_3SO_3H	CH_3SO_3H	Non-redox doping	10.7
	AsF_5	AsF_5	Vapor phase doping	57
Poly(3-vinylperylene)	ClO_4^-	$(C_4H_9)_4N(ClO_4)$	Electrochemical doping	10^{-5}
	AsF_6^-, PF_6^-, BF_4^-	$C_{16}H_{36}AsF_6N$, $(CH_3)_4N(PF_6)$, $(C_2H_5)_4N(BF_4)$	Electrochemical doping	30–100
	ClO_4^-	$LiClO_4$	Electrochemical doping	65
PPy	Cl^-	NaCl	Electrochemical doping	10
	Polystyrene sulfonate (PSS)/Cl^-	$PSS/FeCl_3$	Solution doping	4
	MeOH	MeOH	Vapor phase doping	0.74
	$C_{20}H_{37}O_4SO_3^-$	$C_{20}H_{37}O_4SO_3Na$	Solution doping	4.5
	$C_{10}H_{15}OSO_3^-$	$C_{10}H_{16}O_4S$	Solution doping	300
PANI	HCl	HCl	Non-redox doping	10
	I_2	I_2	Vapor phase doping	9.3
	BF_4^-	HBF_4	Solution doping	2.3×10^{-1}
PBTTT[a)]	FTS[b)]	$C_8H_4F_{13}SiCl_3$	Vapor phase doping	604 to 1.1×10^3
Poly(2-(3-thienyloxy) ethanesulfonate)	Na_2SO_3	Na_2SO_3	Solution doping	5
PT	Cl^-	$FeCl_3$	Vapor phase doping	10–25
PANI–PPy	ASPB	Anionic spherical polyelectrolyte brushes (ASPB)	Electrochemical doping	8.3

a) Poly(2,5-bis(3-tetradecylthiophen-2-yl)thieno[3,2-*b*]thiophene).
b) Tridecafluoro-(1,1,2,2-tetrahydrooctyl)-trichlorosila.
Source: Le et al. [26]. Licensed under CC BY 4.0.

polymeric structure. Doping/de-doping is a reversible process that is used in many modern applications.

As discussed previously, the electrical conductivity of conjugated polymers is strongly dependent on the doping level, and achieving maximum conductivity can be a technical challenge in the research community. Therefore, a number of doping methods have been evaluated and developed for conjugated polymers, including electrochemical doping, chemical doping, *in situ* doping, radiation-induced doping or photodoping, non-redox doping, and charge-injection doping, which are summarized in Table 1.3 [53–55]. Electrochemical and chemical doping techniques are popular in the literature because they involve simple procedures at low cost. Chemical doping can be performed directly by vapor-phase/gaseous or solution pathways. For vapor-phase doping, polymers generally are exposed to the gas phase of dopant compounds, such as bromine, iodine, chlorine, or AsF_5 in a closed system, in which the vapor pressure, temperature, and reaction time determine the final conductivity. Solution doping is accomplished by dipping the solid polymer in a soluble solvent containing dopant ions, such that the original form of the polymer is retained. Doping of conjugated polymers can be electrochemically performed during or after polymerization. By applying appropriate potentials between a conjugated polymer-coated working electrode and counter electrode, a redox reaction takes place at the interface of the material and electrolyte, and ions will diffuse to compensate for the losses at the nearby electrode. This doping method is easy and precisely controls the degree of doping, and is more readily reversible by monitoring the current passed when compared with chemical approaches. However, it is difficult to remove the doped polymer from the electrode and thus apply the process to large-scale fabrication of doped conjugated polymers for industrial applications. Overall, new discoveries in doping processing have led to achieving higher conductivity, in which both n-type and p-type dopants are used for improving the electrical conductivity of organic conjugated systems.

1.2.3 Temperature Dependence

Over the past four decades, there has been remarkable progress in the development of highly conjugated polymers. In highly doped cases, the conductivities of polymers can achieve very high levels comparable to those of their inorganic counterparts. A significant temperature dependence has been observed and investigated for a wide range of conjugated systems, such as polyacetylene, PANI, PPV, and PPy [56, 57]. Based on theoretical perspectives, the relationship between the temperature and conductivity or resistivity of doped conjugated polymers can be exploited in three regimes according to their reduced activation energy (W), as reported by Zabrodskii and Zinov'eva [58] using the following formula.

$$W(T) = -\frac{T[\mathrm{d}\ \ln\ \rho(T)]}{\mathrm{d}T} = \frac{\mathrm{d}(\ln\ \sigma)}{\mathrm{d}(\ln\ T)} \tag{1.4}$$

In the insulating regime, the charge transport mechanism is governed by a variable-range hopping mode near the Fermi level. Therefore, the conductivity (σ)

Table 1.3 Methods used for doping conjugated polymers.

Doping method	Controlled variables	Advantages	Disadvantages
Chemical doping	Vapor pressure, exposure time to dopant	Simple doping process by exposing the sample to a dopant vapor or immersion in a dopant solution	Performed as slowly as possible to avoid inhomogeneous doping. The doping levels obtained are not stable with respect to time
			Unexpected structural distortion may cause electrical conductivity decay
			Doping/de-doping shows low reversibility
Electrochemical doping	Amount of current passed	Doping level can be easily controlled by using an electrochemical cell with a controlled amount of current passed. Doping/de-doping is highly reversible and clean polymer can be retrieved	Unexpected structural distortion may cause electrical conductivity decay
		Can be achieved with many dopant species	
Photo doping	Radiation energy of light beam	Charge carrier is formed without chemical compound (dopant). No distortion of the material structure	Electrical conductivity disappears rapidly when irradiation is discontinued owing to recombination of electrons and holes
Non-redox doping	Protonic acid strength	Number of electrons generally does not change	Depends on the degree of oxidation of conjugated polymers and degree of protonation of the material. Low conductivities are observed for some conjugated polymers
Charge-injection doping	Applying an appropriate potential on the polymer structure	Does not generate counter ions. Minimized distortion	Coulombic interaction between charge and dopant ions is very strong and can lead to changes in the energetics of the system

Source: Le et al. [26]. Licensed under CC BY 4.0.

follows Mott's law [59]:

$$\sigma = \sigma_0 \exp\left(\frac{T_0}{T}\right)^{1/(n+1)} \tag{1.5}$$

where σ_0 and T_0 are constants, and n is the dimensional conduction. Here, the resistivity is activated, and the activation energy has a negative temperature coefficient, which can be described by [60]

$$\log_{10} W(T) = A - x \log_{10} T \tag{1.6}$$

where $A = x\log_{10} T_0 + \log_{10} x$ [60]. Using Eq. (1.6), the slope x and the dimensionality of the sample can be observed.

At the critical boundary of the metallic-insulating regime, the activation energy is independent of temperature, and the slope in Eq. (1.6) becomes zero. The conductivity thus obeys a power law:

$$\sigma(T) = aT^{\beta} \tag{1.7}$$

Here, a is a microscopic length. Equation (1.7) is valid when β is in the range of 1/3 to 1. If β is higher than 1 or lower than 1/3, the system is dominated by insulating or metallic sites of the metallic–insulating transition, respectively. In the case of the metallic regime, $W(T)$ has a positive temperature coefficient and the conductivity at zero temperature is finite ($T \to 0$). Therefore, the conductivity in this regime is expressed by

$$\sigma = \sigma_0 + mT^{1/2} + BT^{p/2}\ (1.7), \qquad m = \alpha\left[\frac{4}{3} - \gamma\left(\frac{3F_\sigma}{2}\right)\right] \tag{1.8}$$

Here, σ_0 is the conductivity at zero-temperature, B is a constant of the localization effects, γF_σ is the interaction parameter, α is the diffusion coefficient parameter, and p is the value of the electron–phonon/electron–electron scattering rate calculated as $p = 3, 2$, and $3/2$ for inelastic electron–electron scattering, weakly disordered, and strongly disordered material, respectively. Localization and interaction induce conductivity via the "$mT^{1/2} + BT^{p/2}$" term [44, 46, 61]. In the case of disordered materials, charge transport at low temperatures is strongly affected by electron–electron interactions. Ahlskog et al. [60] have clearly reviewed the temperature dependence of conductivity in various regimes for conjugated polymers, which can be summarized in Table 1.4, for common, doped conjugated polymers.

It is acknowledged that the conductivity of conventional metals increases with a reduction in temperature, in contrast to the conductivity of doped conjugated polymers, in which conductivity increases with an increase in temperature. Some previous pioneering works have observed that the conductivity of doped conjugated polymers depends heavily on temperature at low doping levels but weakens at high doping levels [62, 63]. Therefore, the conductivity of doped conjugated polymers is strongly affected by the phonon-assisted hopping mechanism at localized states, which is affected by material imperfections or tunneling between metallic regions [30]. For instance, Roth et al. [63, 64] characterized the temperature dependence of the DC conductivity based on a study of iodine-doped polyacetylene by monitoring doping levels. They observed that there was a dramatic increase in

Table 1.4 σ (300 K) and $\rho_r = [\rho(1.3\text{ K})/\rho(300\text{ K})]$ values for several representative conjugated polymers in the metallic, critical, and insulating regimes.

Doped conjugated polymers	Metallic		Critical		Insulating	
	ρ_r	σ (S/cm)	ρ_r	σ (S/cm)	ρ_r	σ (S/cm)
Polyacetylene-I_2	<10	>5000	10–20	$3–5\times10^4$	>20	<3000
Polyacetylene-I_2	<5	$>5\times10^4$	9.8–165	$2–5\times10^4$	>400	$<2\times10^4$
Polyacetylene-$FeCl_3$	<2	$>2\times10^4$	2.6–11.4	$1–2\times10^4$	>27	$<10^4$
PPV-AsF_5	<5	300–2400	9.7–34	100–300	>50	<100
PPV-H_2SO_4	<2	$>4\times10^3–10^4$	4.7–27	1000–4000	>60	<1000
PPy	<2	300–400	2–10	200–300	>10	<200
PANI	<2	250–350	2–5	200–250	>10	<200

Source: Ahlskog et al. [60]. © 1997, IOP Publishing.

conductivity for low doping level samples as the temperature increased, whereas highly doped samples exhibited a small increase in conductivity. In another study, Aleshin et al. [65] investigated the temperature dependence of the DC conductivity of PF_6-doped poly(3,4-ethylenedioxythiophene) (PEDOT). The conductivity exhibited a very weak temperature dependence of $\rho_r = \left[\frac{\rho(1.4\text{ K})}{\rho(291\text{ K})}\right] = 1.5 - 2.8$, which suggests that the material lies on the metallic side of the metallic-insulating transition. It is recognized that the resistivity increases as the temperature drops to 10 K. At lower temperatures, there is a small decrease in resistivity, which is similar to conventional metal, owing to electron–electron interactions at low temperatures. Recently, camphor sulfonic acid-doped PANI was shown to exhibit metallic properties similar to conventional metals, with high conductivity in excess of 1000 S/cm at room temperature [66]. The resistivity weakened as the temperature decreased monotonically over a large range, from 300 to 5 K with $\rho_r = \left[\frac{\rho(5\text{ K})}{\rho(300\text{ K})}\right] \approx 0.4$. This discovery indicates that camphor sulfonic acid-doped PANI lies squarely on the metallic side of the metallic–insulator transition, in which the doped polymer exhibits conventional metallic behavior over a wide range of temperatures. Therefore, doped conjugated polymers can be used in many electronic applications as metallic materials.

1.3 Electrochemical Properties

1.3.1 Reversible Oxidation/Reduction Process and Charge Storage Behavior

Doping causes some basic changes (e.g. from benzoid to quinoid type) in the geometric structure of a polymer, which affects the generation of charge carriers. However, the initial structure can be rehabilitated by converting the polymer back to its undoped form through a de-doping process. In electrochemistry,

doping/de-doping of conjugated polymers is reversible and corresponds to the oxidation/reduction process, which forms the basic concept of a charge/discharge cycle in polymer-based lithium-ion batteries and electrochemical capacitors. In general, p-type doping of conjugated polymers is the electrooxidation process in which electrons are removed from the polymer backbone and the lost electrons are balanced by the insertion of counter-anions from the electrolyte into the polymer skeleton. In contrast, n-type doping of conjugated polymers corresponds to the electro-reduction process, in which electrons are injected into the polymer matrix and counter-cations are added to readjust the overall electrical charge. For instance, electrooxidation and electro-reduction corresponding to the charge/discharge process of p-type and n-type doped PANI by sulfuric acid and lithium ions can be expressed as follows:

Electrooxidation (charging process): $\mathrm{PANI} + n\mathrm{SO_4^{2-}} \rightarrow \mathrm{PANI^{2n+}} : n\mathrm{SO_4^{2-}} + 2n\mathrm{e}$

Electro-reduction (discharging process): $\mathrm{PANI^{2n+}} : n\mathrm{SO_4^{2-}} + 2n\mathrm{e} \rightarrow \mathrm{PANI} + n\mathrm{SO_4^{2-}}$

Electrooxidation (charging process): $\mathrm{CP^{n-}(Li^+)}_n + n\mathrm{e} \rightarrow n\mathrm{CP} + n\mathrm{Li^+}$

Electro-reduction (discharging process): $n\mathrm{CP} + n\mathrm{Li^+} \rightarrow \mathrm{CP^{n-}(Li^+)}_n + n\mathrm{e}$

The insertion/deinsertion of doping ions may cause a huge volume expansion, resulting in degrading the structure of bulk electrode materials. The use of conjugated polymers as the electrode material can provide free void volume in the electrode to prevent the so-called pulverization. Both pristine and doped conjugated polymers can be used as materials for anodes, cathodes, or both for energy storage devices. In general, cyclic voltammetry (CV) is a common technique used to characterize the redox reaction and investigate electron transfer kinetics during doping and de-doping of conjugated polymers. Under an applied potential and a constant scan rate, counter ions will be absorbed and de-absorbed on the polymer during the doping and de-doping processes through forward and backward scans, respectively. The oxidation step causes the polymer chain to become negatively charged, whereas the reduction step results in a positively charged form. The peak current density (A) of adsorbed species from the CV for the reversible system is then given by

$$i = n^2F^2A\Gamma v\left[\frac{\exp\theta}{RT(1+\exp\theta)^2}\right] \tag{1.9}$$

where n is the electron number, F is the Faraday constant (C/mol), v is the scan rate (V/s), Γ is the surface coverage of oxidized or reduced states (mol/cm^2), A is the active electrode area (cm^2), and $\theta = (nF/RT)(E-E)^\circ$. At the peak location, one-electron redox processes produce a symmetrical, cyclic voltammogram with $E - E^\circ = 0$ and $i_\mathrm{R} = -i_0$, and the current can be simplified as

$$i = \frac{n^2F^2A\Gamma v}{4RT} \tag{1.10}$$

It is noted here that the peak current density is proportional to the potential of the scan rate, which can only be applied to ultrathin film conjugated polymers and dopant ions with minor diffusion coefficients. For instance, Diaz et al. investigated the one-electron redox process through the electro-polymerization reaction of

BF_4-doped PPy thin film [67]. The cyclic voltammograms exhibit symmetrical redox peaks in the range of an applied potential of −0.4 and +0.3 V and scan rate from 10 to 100 mV/s. The current increase is proportional to an increase in the scan rate, and the cyclic voltammograms are not affected by diffusion due to stirring conditions. It is observed that after the polymer transferred from neutral to oxidized states, its color changed from yellow to black. Figure 1.7 indicates that the oxidation peaks exhibit a small negative potential shift and that the reduction peaks become more positive when the scan rate is increased [68]. The redox reactions may not take place completely owing to the limitation of the reaction time at high scan rates, and thus severe kinetic limitations may contribute to charge transfer at high scan rates. With increasing thickness polymer films or dopant ion size, the electrochemical process is affected by diffusion. Therefore, the symmetrical form of the voltammogram changes to an asymmetrical shape and the peak current density is then proportional to $v^{1/2}$.

In multi-electron redox processes, more than one pair of redox peaks can be observed in cyclic voltammograms, which are presented in Figure 1.8 for reversible p-doping of PANI. Two oxidation peaks appear at 0.72 and 0.31 V when the polymer undergoes a doping process at an applied scan rate of 50 mV/s. Two reduction peaks

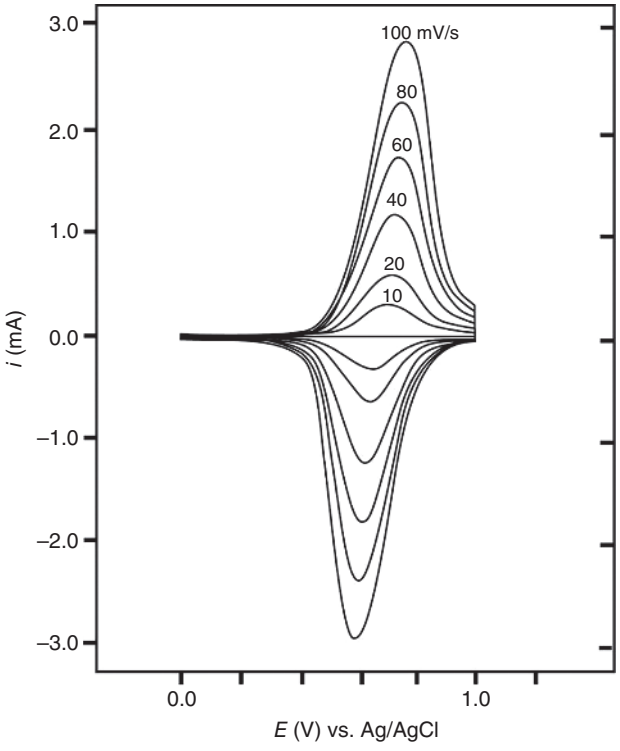

Figure 1.7 Cyclic voltammograms of a poly(*N*-phenyl-1-naphthylamine) film on Pt in 1 M $LiClO_4/CH_3CN$ solution at different scanning rates. Source: Guay et al. [68]. © 1990, American Chemical Society.

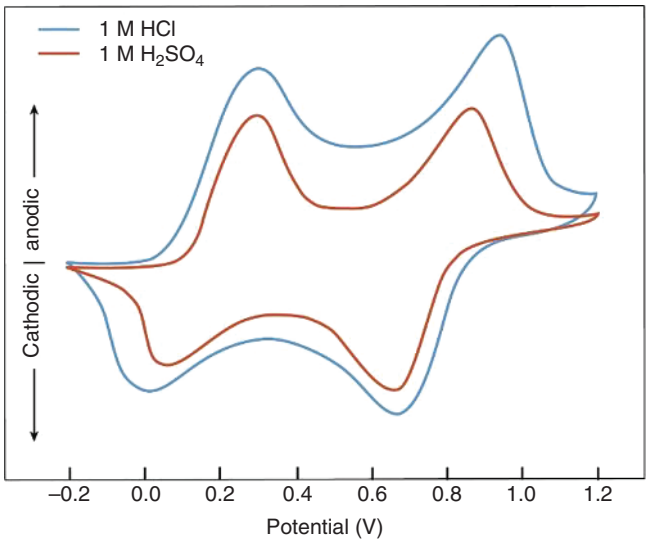

Figure 1.8 Cyclic voltammetry (CV) curves of a polyaniline (PANI) film doped with hydrochloric acid or sulfuric acid at the same potential scan rate of 50 mV/s. Source: Le et al. [26]. Licensed under CC BY 4.0.

are located at 0.48 and 0.09 V through the backward scan, which corresponds to de-doping of PANI. It is recognized that PANI exhibits different electrochemical behaviors when using different types of acid electrolytes, such as sulfuric and hydrochloric acid, which may result from disparities in the charges and sizes of counter-ions. Protons and anions are generated when dispersing hydrochloric and sulfuric acids into water, respectively. The main difference between the two acids is attributed to the disparities between SO_4^{2-} and Cl^- anions. The radius of (SO_4^{2-}) is 0.258 nm, which is higher than that of Cl^- (0.181 nm), where an increase of electrons in the shell is present, and thus the larger (SO_4^{2-}) ions may have less efficient diffusion into the polymer matrix than the smaller (Cl^-) ions under electrochemical doping. Alternatively, the type of dopant is also believed to affect the electrical conductivity of the doped polymer. Here, hydrochloric acid-doped PANI exhibits better electrical conductivity, which implies that the diffusion of dopant ions is a significant factor in the development of high conductivity of the conjugated polymer electrode based on electrochemistry.

As discussed previously, the redox reactions of conjugated polymers represent a reversible and stable process over a range of applied potentials. However, when scanning conjugated polymers at very high potentials, the structure of the electrode material is degraded, leading to loss of its electro-activity and a decrease in the potential window available for reversible reactions. This phenomenon has been observed in the early stages of development of conjugated polymers and is referred to as overoxidation [69]. Overoxidation is an irreversible reaction and its mechanism is not clearly understood. Beck and coworkers observed the overoxidation of PPy and polythiophene, and speculated that the contamination of strong nucleophiles

such as OH^-, CN^-, and Br^- in an electrolyte solution may be added to the polymer matrix upon strong polarization, or radical cations may be added, therefore causing polymer destruction and irreversible oxidation with peak potentials ranging from 1.8 to 2.2 V [69–71]. The electrical conductivity of the doped polymer will be destroyed and the polymer will suddenly become an insulator again. Lewis et al. found that the overoxidation of PPy appeared at a potential as low as 0.65 V, and that the overoxidation potential highly depended on the pH of the supporting electrolyte [72]. In some cases, there was no overoxidation detected when the pH approached zero owing to the high stability of the polymer at this pH [72, 73]. Hence, an appropriate selection of electrolyte, solvent, and redox potential window is necessary to retain the high reversible redox reaction of conjugated polymers, which has led to proposals for many practical applications.

1.3.2 Swelling and De-swelling Behavior

The reversible redox reaction of conjugated polymers can be associated with high volumetric changes in the dimensions of conjugated polymers [74–76]. Swelling and de-swelling phenomena in conjugated polymers have been reported as their state switches from the oxidized to the reduced form, which provide the basis for a new generation of actuator applications. Therefore, many studies have been performed to evaluate the volume changes of conjugated polymers during the redox process, and different mechanisms have been proposed. Kertész et al. found that charge transfer correlates with the increase/decrease in the carbon length and the carbon angle of the polymer (change of geometry) when it receives or loses electrons during the doping/de-doping process [77]. This leads to a change in the intrinsic conformation of the polymer skeleton. On the other hand, it is acknowledged that the movement of counter-ions during the charge balancing process may affect the volume change of the polymer system owing to the occupation/displacement of ions in the polymer matrix. This may be associated with the spontaneous diffusion of solvent molecules into the region of higher concentration of dopant-ions/dopant-ion concentrations in order to equalize concentrations both inside and outside of the polymer matrix. In other words, the movement of the solvent may change the arrangement and concentration of ions in the polymer matrix and may lead to the formation of a semipermeable membrane and its corresponding osmotic pressure. This phenomenon has been reported as an osmotic expansion, which contributes to the total volume change of a conjugated polymer and underlies the primary concept for the development of polymer actuators (Figure 1.9).

In summary, the mechanism of swelling/de-swelling or actuation in conjugated polymers is attributed to a change in the intrinsic conformation of the polymer skeleton and osmotic expansion of the polymer phase due to ions and solvent [78]. The actuation of conjugated polymers can be monitored by a chemical or electrochemical process [79]. In principle, the typical mechanism of the electrochemical actuation in conjugated polymers is described in Figure 1.10. When the conjugated polymer undergoes the oxidation process, electrons are removed, which leads to the formation of positive-charge polarons. To compensate for the charge loss, small anions

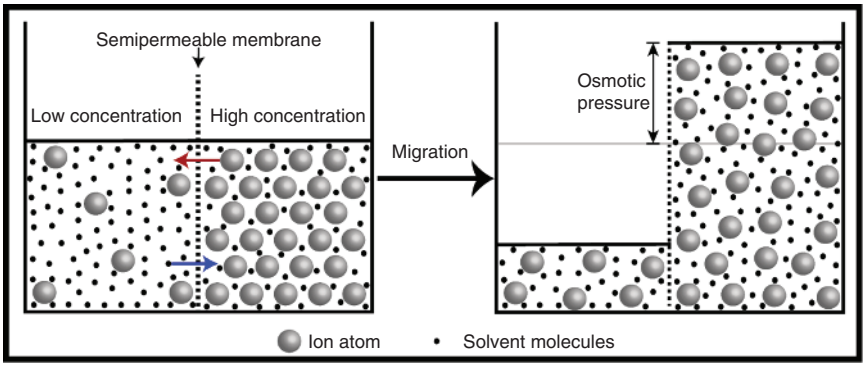

Figure 1.9 Effect of osmotic pressure when driving fluid flow across a membrane.

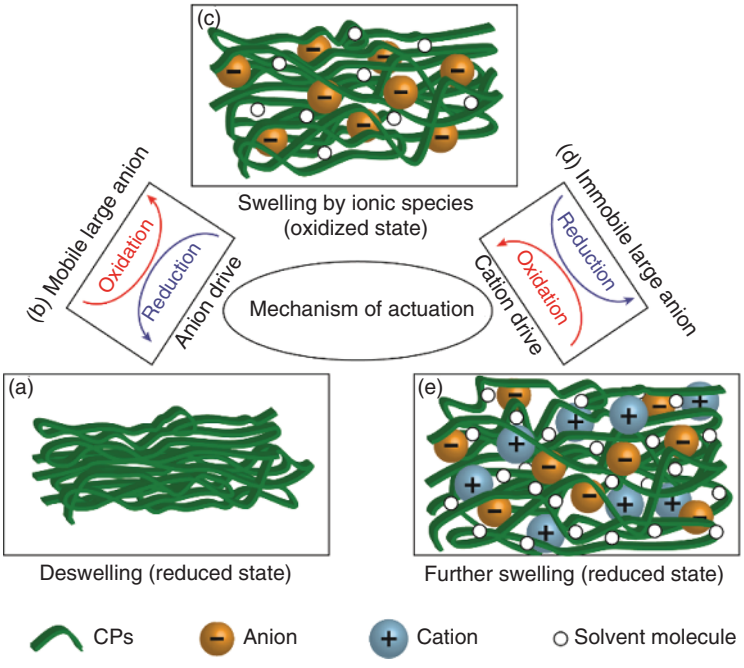

Figure 1.10 Mechanism of electrochemo-mechanical actuation in conjugated polymers. Source: Le et al. [26]. Licensed under CC BY 4.0.

then move into the polymer matrix and create ionic bonds with the polymer backbone, resulting in a small increase of the polymer volume. These anions can be dislodged from the polymer matrix when it is reduced to its initial state by applying a negative voltage (Figure 1.10a–c). In general, p-doping is associated with the anion-driven actuation and intrinsic polymer conformation change which cause swelling through oxidation and de-swelling through reduction [80].

However, full ejection can only be observed for small dopant-ions. When the dopant anion size is large enough, such as for dodecylbenzene sulfonic acid, poly(4-styrenesulfonate), and polyvinylsulfonate, the anions are immobilized and are permanently trapped inside the polymer matrix. Charge compensation during the reduction step then occurs through the affiliation of cations from the electrolyte and causes further expansion (Figure 1.10c–e). This phenomenon is coined in this paper as "cation-driven actuation." At each step of incorporation of ions into the polymer matrix, the ions in motion cause a large, different concentration inside and outside of the polymer matrix. Hence, solvent molecules move in the polymer matrix to neutralize the anion or cation contraction, and the resulting osmotic expansion contributes to the total volume change of the polymer during actuation. This has been confirmed by several groups through observations of expansion reduction based on an increase of electrolytes using electrochemical quartz crystal microbalance and optical beam deflection studies [81–83]. Bay et al. investigated the effects of dopant ions and solvent molecules in an electrolyte solution on the expansion/contraction on dodecylbenzene sulfonate doped PPy [78]. The expansion was found to be reduced by 30% when the concentration of dopant ions in the electrolyte increased from 0.1 to 1.0 M. Similar results were also obtained by Aydemir et al. and Maw et al. [84, 85], suggesting that the movement of the solvent is associated with the concentration of ions in the polymer matrix and electrolyte solution during the redox reaction [75].

Consequently, conjugated polymer actuation is determined by the microstructures of the polymer and type/concentration of dopant and electrolyte. In addition to promoting the potential of those significant factors, it is necessary to develop more advanced actuating systems to achieve high-performance soft actuators based on conjugated polymer. To date, several notable systems have been introduced, such as out-of-plane actuators, linear actuators, and bilayer–trilayer actuators [79].

1.3.3 Electrochromism

It is acknowledged that the reversible doping/de-doping process of conjugated polymer is induced by oxidation/reduction processes. Such reversible redox processes cause a visible change of color in conjugated polymers and this phenomenon is known as electrochromism. This exceptional property of conjugated polymers has attracted global attention for various electrochromic applications such as smart windows, electrochromic displays, and rearview mirrors [86–88]. Both the energy gap and dopant are believed to mutually instigate the color conversion of conjugated polymers. The insertion/de-insertion of dopant ions via doping/de-doping induces the reorganization of the polymer's electronic structure, which results in a reduced energy gap for possible π–π^* transitions. Furthermore, the formation of sub-bands by charge carriers such as polarons and bipolarons modulates the absorbance (new band gap) of the conjugated polymers, leading to the change in their color. Doped conjugated polymer thin films show strong absorption spectra in the visible region, whereas pristine or undoped conjugated polymer thin films are colorless and transparent owing to the high energy gap (>3.0 eV). In the case when

un-doped conjugated polymers possess a lower band gap of approximately 2.0 eV, they can absorb visible spectra and exhibit various colors in this state. However, their absorption/emission in the doped state can shift to the near-infrared region because of the lower band gap of the doped polymer [86].

Conjugated polymers can display variations in color for different redox states. As a notable example, PANI exhibits color changes from transparent yellow to green, blue, and violet for various doped states (Figure 1.11). These electrochromic forms are caused by the protonation/deprotonation process or/and the insertion/de-insertion of dopant ions through p-doping of PANI using the CV technique in salt, acid, and organic solvents. In this case, heteroatoms such as nitrogen play a critical role as the injection sites for anions or protons in order to generate radical cations/doped forms [85, 86]. Their color change and protonation/redox states are clearly illustrated in Figure 1.11. Similarly, by the complexation of conjugated polymers, absorption spectra can be upgraded from the visible to the near-infrared and infrared regions [89]. The switching time of the color variations strongly depends on the migration velocities of protons/dopant ions throughout the polymer matrix. Hence, the electrochromic properties of conjugated polymers depend on the size (discuss in Section 1.4), the pH of the electrolyte solution, redox capability, temperature, and the chemical structure of the polymer. In order to extend the use of conjugated polymers to the next generation of electrochromic devices, the properties of conjugated polymers must be further improved to fulfill the standard requirements of the devices, such as long lifespan, high color contrast, and rapid color change switching.

1.4 Optical Properties

The optical properties of conjugated polymers have largely motivated their industrial applications in optoelectronics and photonics, including light-emitting diodes, solar cells, and field-effect transistors. In general, the optical properties of these materials reflect their geometry and electronic structure, and the materials mainly respond to light by the absorption and emission characteristics of either pristine or doped materials. These properties are strongly dependent on the size, morphology, doping state, and properties of conjugated systems. Therefore, understanding the photophysical properties and charge transport under light excitation should arouse great interest in the development of conjugated polymers for the next generation of optoelectronic, photocatalyst, and imaging and sensing applications. The evolution of the band gap structure and/or optical properties through the introduction of doping has already been discussed in Sections 1.3 and 1.4.3. In this section, the optical properties of conjugated polymers are mainly evaluated based on their inherent structure.

1.4.1 Band Gap of Conjugated Polymers

In general, the electronic band structure is a key parameter for understanding the mechanism of an organic conjugated system used for optoelectronic applications.

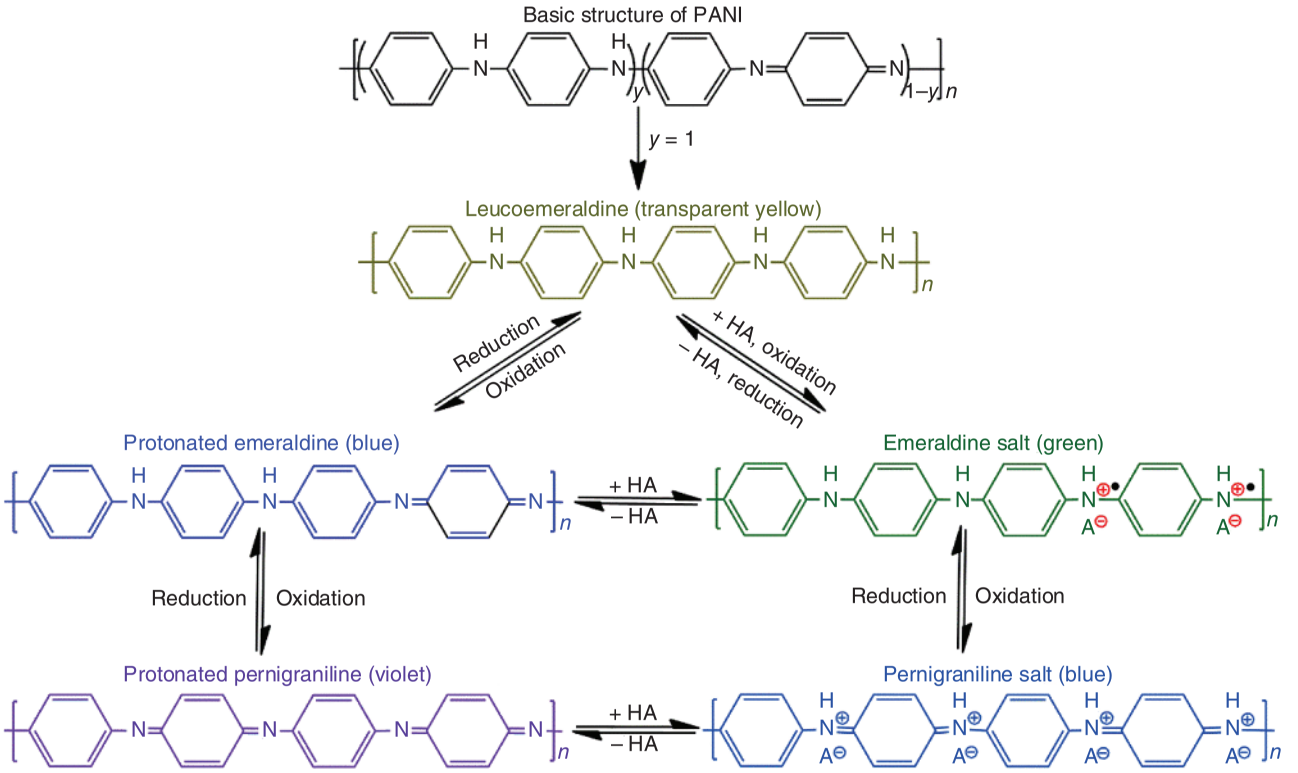

Figure 1.11 Different redox/protonation states and colors of PANI. Source: Le et al. [26]. Licensed under CC BY 4.0.

It is acknowledged that conjugated polymers exhibit similar **electronic band gap** properties as conventional semiconductors along with electron–electron and electron–hole coupling (i.e. a three-dimensional band structure) [90]. The origin of the band gap in conjugated polymers comes from the interchange of single and double bonds in their structure, where a π-electron from the ground state (HOMO) can absorb a photon and jump into the excited π^* state (LUMO), which leaves behind a positively charged hole. Electrons and holes are bonded to each other by Coulomb interaction, forming a neutral quasiparticle, namely, an exciton. The attraction between electron–hole results in the creation of an exciton band below the conduction band threshold [91]. The new excited state is coined the **optical band gap** (E_{opt}) and the exciton binding energy ($E_b = E_g - E_{opt}$) is in the range of 0.5–1.0 eV for various conjugated polymers (Figure 1.12) [91]. Finally, electrons and holes tend to recombine to form the initial form and yield an energy decay **through the radiative or non-radiative process**. Conjugated polymers in solid and liquid phases are characterized by weak intermolecular and strong intramolecular interactions, respectively. Thus, two different forms of excitons, i.e. intrachain and interchain (including both single and triplet excitons), have been identified in π-conjugations along sections of the polymer skeleton resulting from the delocalization of the π-electron system. Among them, interchain excitons are generated by the coupling of two nearby intrachains derived from two different polymer chains, or are derived by single-chain folding in polymer nanoparticles, films, or coiled configurations. This mechanism is responsible for electron delocalization between polymer chains, thus causing a reduction in the band gap of the solid-state material and nanoparticles, leading to a three-dimensional band structure (**interchain band gap**). As a result, both singlets and triplets are thus formed in the intrachain and interchain [92]. It is noted that conjugated polymers also exhibit a similar size dependence regarding optical properties as other nanostructured semiconductors, which refers to the extent of **π-conjugation or conjugation length in terms**

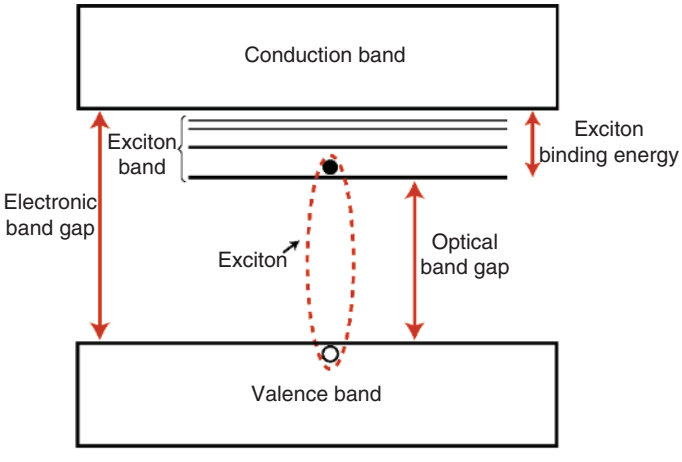

Figure 1.12 Electronic band gap structure and exciton levels formed in conjugated polymers.

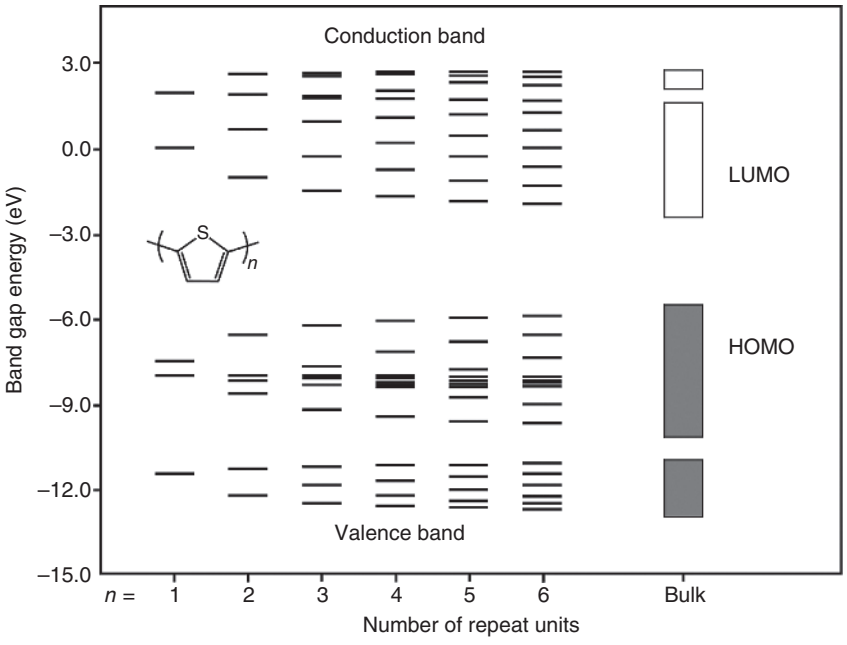

Figure 1.13 Band gap evolution of polythiophene as conjugation length increases. Source: Salzner et al. [93]. © 1998, Elsevier.

of bond length and length of a conjugation chain. The quantum size effects of conjugated polymers originate from the delocalization of π-electrons in the repeating units along the polymer chain. Representatively, Figure 1.13 shows the band gap evolution for polythiophene with increasing numbers of monomer units. When the monomers units increase, the number of π-electrons in the chain increases allows a greater number of atomic orbitals in the overlapping region. The total number of molecular orbitals from both bonding and antibonding is increased along with the width of the energy band. This causes a lower band gap between the conductance band and valence band in larger polymers or bulk materials, known as quantum confinement at the nanoscale. Therefore, the band gap of conjugated polymers (the HOMO–LUMO gap) increases with the decrease of the conjugation length. Another specificity of non-degenerate ground polymers, namely, **planarity** [94] arising from torsional strain, has been considered as an additional factor which limits the delocalization of π-electrons along the backbone, and is thus partially responsible for the larger band gap as the dihedral angle increases (reduced planarity) [95]. It is believed that the presence of heteroatoms in the aromatic system, electron withdrawing and electron donating substituents, and aromaticity determine the electronic and optical properties of conjugated polymers. **Different heteroatoms or substituent** groups contribute to the changes of the optical properties in conjugated polymers, defining the material's electron affinity. For example, heteroatoms have higher electron affinities and tend to decrease the delocalization of π-electrons along the polymer backbone, resulting in lowering

of the band gap. Patra et al. confirmed the effect of heteroatoms (S and Se) based on density functional theory (DFT) and optical studies of polyselenophenes and polythiophenes. The presence of S or thieno-fused aromatic units leads to a decrease of 0.2 eV in the band gap compared with Se or seleno-fused units because sulfur has higher electron affinity than selenium (2.073 eV vs. 2.021 eV). With the larger electron affinity of 0.22 eV to S, NH^- induces a larger band gap of 3.1 eV in PPy vs. polythiophene (2.0 eV) [96]. **In the case of aromaticity**, the overlapping p_z-*or*bitals of π-electrons within these systems could offer different forms, such as aromatic and quinoid (resonance structures). Aromaticity causes π-electrons to be confined within the ring, and limits electron delocalization throughout the polymer backbone under the resonance effect, thus resulting in a larger band gap.

In summary, the single photo-excitation configuration of conjugated polymers causes the jump of an electron from the valance band to the conductance band, and the band gap of a π-conjugated system is the linear combination of the band gaps derived from **interchains** and **intrachains** affected by the following:

- Conjugation length,
- Planarity,
- Heteroatoms in the aromatic system and/or electron-withdrawing and electron-donating substituents, and
- Aromaticity/resonance structure.

Therefore, the band gap and optical properties of conjugated polymers are strongly affected by their chemical structure and morphological characteristics, such as the chain conformation, aggregation state, shape, and size of the polymers.

1.4.2 Absorption and Emission

In conjugated polymers, the chemical structure, conformational order, and overall nanostructure are known to have a significant effect on the electronic band structure, and thereby determine the absorption and emission spectra (or emission colors). Upon photoexcitation by a sufficiently excited photon, an electron is promoted from the HOMO (the π band) to the LUMO (the π^* band) to form an exciton. According to the orientation of spin, a singlet or triplet exciton can be defined. If the electrons in the excited state have the same spin state as in the ground state, they are considered singlet excitons. In contrast, if an excited state electron has the same spin orientation as another unpaired electron (or the opposite spin state as it had in the ground state), it is called a triplet exciton. Depending on the energy of photon excitation, the different excited states can be described by a Jablonski diagram (Figure 1.14a). The singlet ground states are denoted as $S_{0,}$ and the different singlet excited states are defined as S_1, S_2, and S_3, respectively. Similarly, triplet excited states are presented as T_1, T_2, and T_3, and each electronic level has a distinct vibrational energy. The excited state electrons can migrate from a high energy level to a lower energy level by internal conversion, crossing, and relaxation processes. Consequently, an electron can return to the ground state through radiative recombination or unwanted pathway – non-radiative recombination. Radiative recombination is

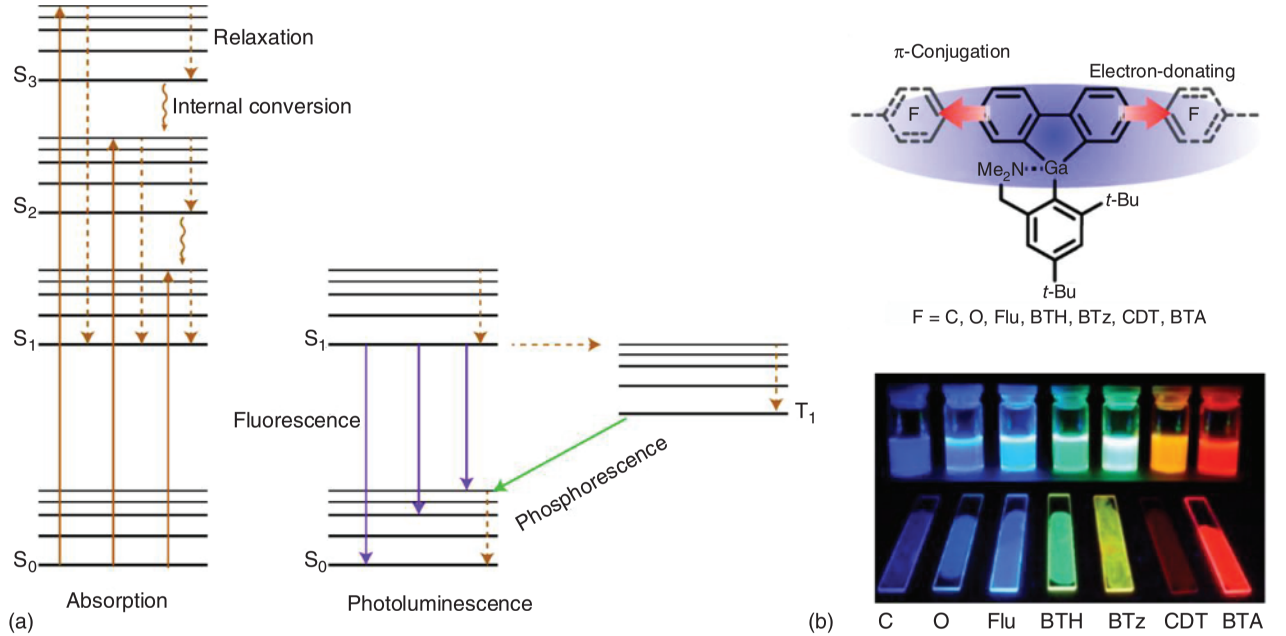

Figure 1.14 (a) Jablonski energy diagram demonstrates the energy levels of conjugated polymers for the quantum mechanical processes of absorption, fluorescence, and phosphorescence. (b) Chemical structure and photoluminescence images of poly-GafC, poly-GafO, poly-GafFlu, poly-GafBTH, poly-GafBTz, poly-GafCDT, and poly-GafBTA, under UV light (365 nm). Source: Based on Matsumoto et al. Reprinted with permission from [97]. Copyright 1990, American Chemical Society.

one of the most useful processes in conjugated polymers to generate **photoluminescence** with red-shift or longer wavelengths in comparison with absorbed light. The emitted light derived from the singlet excitons is referred to as **fluorescence**, while light derived from triplet excitons is referred to as **phosphorescence**, which normally occurs over longer time scales and at a lower intensity than fluorescence. The emission properties of conjugated polymers such as PPVs were discovered in the early 1990s and were attributed to the delocalization of π-electrons along the polymer backbone [98]. It was reported that PPVs could emit a light over a large region from green to yellow, which suggested that polymers can be used for the development of light-emitting diodes. It is now known that the chemical structure, chain conformation, and the size define color emission via the band gap of conjugated polymers.

Different chemical structures have been designed to tune the color from blue to red regions for different conjugated polymers, such as poly(9,9-dioctylfluorenyl-2,7-diyl), poly[(9,9-dioctyl-2,7-divinylene-fluorenylene)-alt-*co*-(2-methoxy-5-(2-ethylhexyloxy)-1,4-phenylene)], poly[(9,9-dioctylfluorenyl-2,7-diyl)-*co*-(1,4-benzo-(2,1′,3)-thiadiazole)], poly[2-methoxy-5-(2-ethylhexyloxy)-1,4-phenylenevinylene], poly(3-alkylthiophene), poly(*p*-phenylene), and poly(2,5-di(3=,7=-dimethyloctyl) phenylene-1,4-ethynylene). The photoluminescence quantum yield of conjugated polymers can range from 20% such as for polythiophene dots up to 80% in the case of polyparaphenylene and polyfluorene nanostructures [99–102]. The absorption and emission spectra depend on the molecule length of conjugated polymers. However, the absorption intensity and photoluminescence quantum yield are in inverse proportion to the length of the polymer chain. Hou et al. [103] observed that the photoluminescence quantum yield decreases for the larger conjugated polymer molecules, namely poly[2-methoxy-5-(2-ethylhexyloxy)-1,4-phenylenevinylene]. Simultaneous absorption and emission measurements on single molecules have proven that the quenching of photoluminescence occurs by an increase in the conformation defects, which trap electrons as the prolongation of the polymer chain increases (affect the polymer folding and packing during the nanostructure preparation process) [103, 104]. Matsumoto et al. [97] synthesized full visible colors of conjugated polymers using gallafluorene (Gaf)-containing various comonomers such as 2,5-didecylbenzene-1,4-diboronic acid bis-(pinacol) ester (**C**), 2,5-didecyloxybenzene-1,4-diboronic acid bis(pinacol)ester (**O**), 2,7-bis(4,4,5,5-tetramethyl-1,3,2-dioxaborolan-2-yl)-9,9-didodecylfluorene (**Flu**), 4,4′-didodecyl-2,2′-bithiophene-5,5′-diboronic acid bis(pinacol)ester (**BTH**), 4,7-bis(trimethylsilylethynyl)-2-(2-decyltetradecyl)-2*H*-benzo[*d*]-[1,2,3]triazole (**BTz),** 2,6-bis-(4,4,5,5-tetramethyl-1,3,2-dioxaborolan-2-yl)-4,4-dioctyl-4*H*-cyclopenta[2,1-*b*:3,4-*b*′]dithiophene (**CDT**), and 4,7-bis[3-hexyl-5-(trimethylstannyl)thiophen-2-yl]benzo[*c*]-[2,1,3]thiadiazole (**BTA**). The Gaf unit plays a role as an electron-donor in π-conjugated systems, where the electronic interaction between Gaf and various comonomers leads to different band gaps and results in the display of dark blue, blue, cyan, green, yellow, orange, or red colors (Figure 1.14b). Schütze et al. [105] prepared defect-free oligo(phenylene ethynylene)s rods with increased chain length up to 43 repeat units. It was found that the absorption and emission wavelengths red-shifted

with increasing chain length and finally covered a blue region (400–460 nm). Therefore, most of the recent studies have focused on creating different emission colors based on different conjugated polymers and their derivatives along with monitoring chain conformation and chain alignment by controlling the size, aggregation, heteroatoms, and electron-withdrawing and electron-donating substituents.

Along with full visible color tuning, conjugated polymers, as well as their nanostructures, also exhibit high photoluminescence quantum yield, good thermal stability, good absorption, biocompatibility, non-toxicity, and high-functionalization sites, making them promising candidate materials for biology, biomedical, and optoelectronic applications [106]. The main drawback of conjugated polymers is their color instability, which can reduce the life-span of some devices such as light-emitting diodes (LEDs) [107]. Reducing the migration of excitons to defect sites significantly enhances color stability [108, 109]. Further research to understand the mechanism of quenching in conjugated polymers will enable higher performance of conjugated polymers for photoluminescence applications.

1.4.3 Coherent Exciton Diffusion and Energy Transfer

In conjugated polymers, two types of electronic energy transfer have been discovered: intrachain transfer and interchain transfer [110, 111]. The energy transfer occurs by excitons hopping along a conjugated polymer chain or two polymer chains [25]. However, the generated interchain and intrachain excitons in conjugated polymers are governed by electrostatically bound electron–hole pairs and structural defects that prevent the production of a high flow of current in certain cases. This is the result of the low dielectric constant of conjugated polymers, which is in the range of 3–4 [112]. Various electron donor–acceptor systems in terms of p–n heterojunctions have been developed to improve the dissociation of excitons and thus enable a higher energy transfer process, in which appropriate electron donor/acceptor material can aid in breaking the Coulomb attraction (dissociation), which can then allow excitons to diffuse to the interface and produce a photocurrent suitable for photovoltaic applications. Conjugated polymers can be used as electron donor or electron acceptor material according to the device requirements. The charge carriers can be formed by photo-excitation in photovoltaic cells or by charge-injection in organic light emitting diodes. The diffusion of excitons in conjugated polymers playing the role of electron donor–acceptor materials in the conversion process from singlet excitons of the photovoltaic cell is described in Figure 1.15.

The two materials have different ionization energies and electron affinities and thereby create an electrostatic force at the interface. Under the excitation of an appropriate light wavelength, the electrons of the polymer (the donor material) will move to the LUMO and leave holes in the HOMO, forming excitons in the small charged region. When excitons are generated at the interface of the two materials, the electrons will transfer to the higher electron affinitive material and the holes will move to the lower ionization potential material and generate photocurrent.

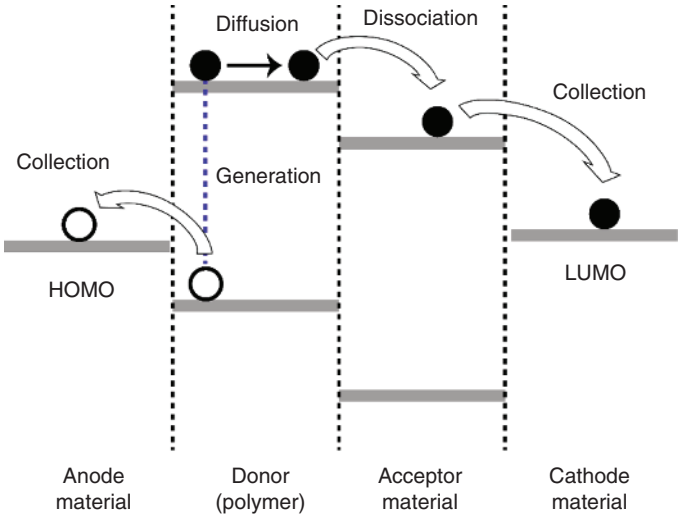

Figure 1.15 Exciton diffusion and energy transfer in conjugated polymers through charge annihilation.

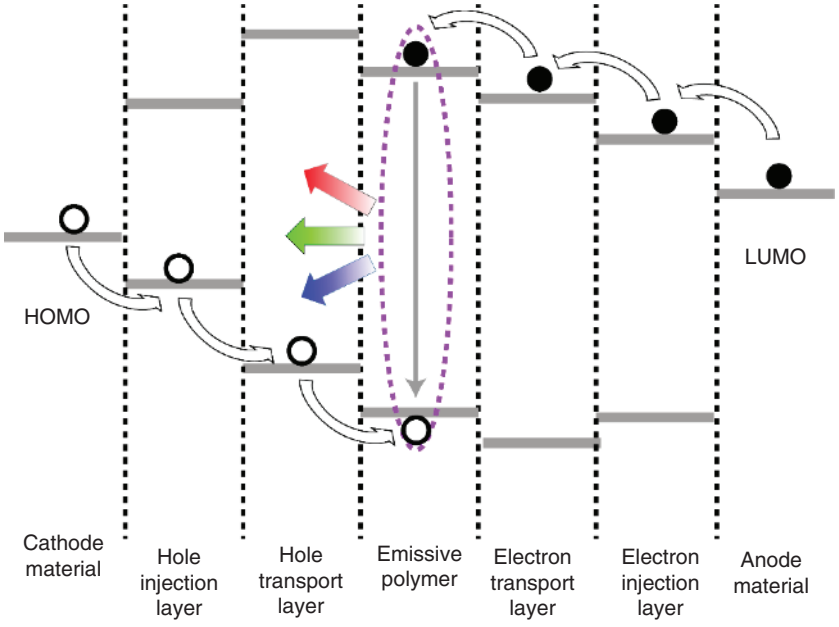

Figure 1.16 Exciton diffusion and energy transfer in conjugated polymer through electron–hole recombination.

Similarly, Figure 1.16 presents the typical energy transfer for hole injection and electron injection conjugated polymer materials in LEDs. Under an applied current between two electrodes, electrons and holes are injected from the anode and cathode electrodes, respectively, and then transfer to the emitting material. Consequently, this leads to the formation of singlet and triplet excitons in the

conjugated polymer (emitting layer) and light is emitted through the recombination mechanism.

It is noted that excitons can be governed in the excited state of conjugated polymers with ratios of 25% and 75% for singlet and triplet states, respectively [113]. Harvesting the light/energy from single excitons leads to a low conversion efficiency owing to a 75% loss caused by the absence of triplet excitons. Therefore, many researchers have attempted to collect both singlet and triplet excitons to maximize efficiency [114, 115]. Many strategies have been introduced, including multiple processes such as **single-triplet energy transfer and singlet fission-triplet energy transfer for photovoltaics,** as well as thermally activated delayed fluorescence, hybridized local and charge-transfer excited state, and triplet-fusion delayed fluorescence, for organic light-emitting diodes (OLEDs) [116–118]. In general, the exciton diffusion length (L_D) of conjugated polymers defines the distance that excitons can diffuse over their lifetime in a presented material [119, 120]. It plays a significant role in many organic optoelectronic devices and can be defined as the root mean square of an exciton's displacement from its initial position (dL_i) during the exciton's lifetime (τ) as

$$L_D = \sqrt{\frac{\sum dL_i^2}{N}} = \sqrt{2ZD\tau} \tag{1.11}$$

where Z is the dimensional number, D is the diffusion coefficient, N is the number of excitons, and i represents an individual exciton. In one-dimensional structures, the factor 2 is usually omitted and the exciton diffusion length can be expressed as

$$L_D = \sqrt{D\tau} \tag{1.12}$$

However, the lifetime of an exciton is ultrafast (<1 ns) and diffusion lengths are less than 20 nm in typical conjugated polymer films, which is less than the optical absorption pass length [121]. Finally, the thin film has less efficiency in absorbing light and only limited excitons are diffused to the interface of the planar heterojunction in photovoltaic devices (low L_D). The bulk heterojunction concept has been used to enhance the diffusion of excitons to the interface by increasing the surface interactions of donor and acceptor materials. In addition, improving the interfacial area between electron donor and acceptor material via nanostructured conjugated polymers (1D, 2D, and 3D) can offer higher quantum conversion efficiencies as compared with thick film or bulk conjugated polymers, as the larger effective area provides better surface interactions and prevents energy losses [122]. In contrast to photovoltaic cells, a larger L_D in OLEDs can cause low luminous efficiency because excitons decay through non-radiative pathways, including oxidation defects and electrodes [123, 124].

Understanding the mechanisms of energy transfer in conjugated polymers including the exciton diffusion pathway(s) and length(s) should improve the performance of conjugated polymers and their nanostructures based on current optoelectronic applications, and their low cost should make them attractive for the next generation of devices.

1.5 Unique Properties at the Nanoscale

First, it is important to note that conjugated polymer nanostructures (CPNs) can show higher conductivities compared to their bulk counterparts. Martin group demonstrated that the conductivity of conjugated polymer nanotubes grown in a template was much higher than that of their bulk counterparts [57]. The enhancement in conductivity was related to the high orientation of the polymer chains nearby the template walls and as a result elongated conjugation length. When the diameter of the nanotube became larger, the conductivity decreased because the portion of the more disordered core would increase. Similar examples showing the size effect of CPNs on the conductivity have been reported [58, 59]. Reducing the dimensions of conjugated polymers into a nanometer scale offers more opportunities to increase the chain orientation, crystallinity, and doping level of the polymer. The transport properties of CPNs are still a subject of great interest and play an important role in fundamental research and industrial application of conjugated polymers.

CPNs have higher surface area and smaller dimensions, enabling them to show more efficient and rapid electrochemical reactions. In addition, at the nanoscale, the morphology of conjugated polymers has a crucial effect on their electrochemical properties. Notably, a recent work by Park et al. demonstrated a correlation between the morphology and electrochemical performance of PANI nanostructures with different aspect ratios (Figure 1.17) [125]. Although all the PANI nanostructures had similar CV curve shapes, the integrated area of the CV curve clearly increased in the order of nanospheres < nanorods < nanofibers. Both anodic (I_{pa}) and cathodic (I_{pc}) peak current densities increased with increasing scan rate, indicating that the electrode kinetics were subject to a surface-controlled redox process. The anodic (E_{pa}) and cathodic (E_{pc}) peak potentials were plotted as a function of the logarithm of the scan rate (v) to calculate the electron transfer coefficient (α) and electron transfer rate constant (k_s) from Laviron's theory [126].

$$E_{pa} = a + \left[\frac{2.303RT}{(1-\alpha)n_{\alpha}F}\right] \log v \tag{1.13}$$

$$E_{pc} = b - \left[\frac{2.303RT}{\alpha n_{\alpha}F}\right] \log v \tag{1.14}$$

$$\log k_s = \alpha \log(1-\alpha) + (1-\alpha) \log \alpha - \alpha(1-\alpha)\frac{nF\Delta E_p}{2.3RT} - \log \frac{RT}{nFv} \tag{1.15}$$

The evaluated α and k_s values were found to be 3.6×10^{-1} to 3.7×10^{-1} s^{-1} and 4.3×10^{-1} s^{-1} for PANI nanofibers, with the latter value being higher than that of nanorods (3.1×10^{-1} s^{-1}) and nanospheres (2.6×10^{-1} s^{-1}), suggesting that the electron transfer capability of the PANI nanostructures strongly depended on their morphological characteristics.

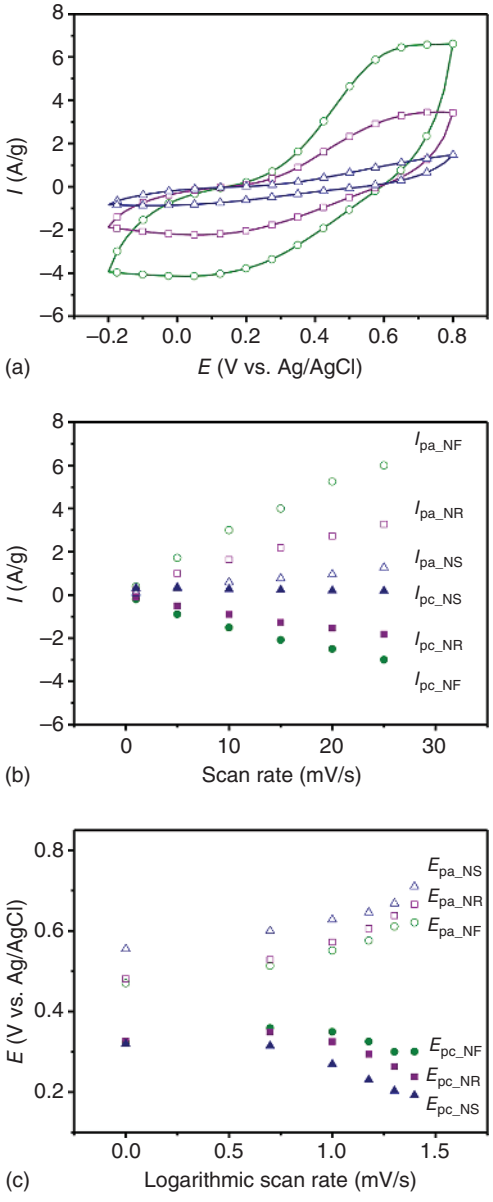

Figure 1.17 CV analysis of PANI nanostructures with three different shapes (nanospheres, NS; nanorods, NR; and nanofibers, NF) performed in a 1 M sulfuric acid dopant solution. (a) Cyclic voltammograms of electrodes consisting of PANI nanostructures at the same scan rate (25 mV/s); (b) plots of the peak current (the anodic peak current, I_{pa}; the cathodic peak current, I_{pc}) vs. the scan rate; and (c) plots of the peak potential (the anodic peak potential, E_{pa}; the cathodic peak potential, E_{pc}) vs. the log of the scan rate. Source: Park et al. [125]. © 2012, American Chemical Society.

1.6 Conclusion

The fundamentals of conjugated polymers as well as their nanostructures, including electrical, electronic, optical, and electrochemical properties, have become more important over the last three decades as the utility of conjugated polymers has been discovered. Deep understanding of these properties will provide opportunities for the development of various applications which directly utilize CPNs. Various

theoretical charge transport models have been proposed for both pristine and doped conjugated polymers. However, there remain challenges to overcome because of several issues associated with polymeric conjugated systems, including structural defects, chain conformation, and interchain interactions. With the aid of novel spectroscopy and simulation methods, extended studies that can determine the correlations between/among doping reaction, color changes, swelling/de-swelling, and conductivity may provide the knowledge that can define the charge transport kinetics/mechanisms for a wide range of conjugated polymers. The conductivity of pristine conjugated polymers dominates the insulator–semiconductor transition and offers unique optical properties, such as absorption and photoluminescence. The electrical conductivity of conjugated polymers can be successfully enhanced by chemical, electrochemical, or photodoping, where both n-type and p-type dopings can be used to activate metallic behaviors in conjugated polymers. The formation of charge carriers (polarons, bipolarons, and solitons), their mobility, and the mobility of excitons in pristine and doped conjugated polymers are strongly affected by the dopant, doping state, and the inherent properties of conjugated systems such as chain conformation, aggregation state, and shape and size of the material. Possessing many advantages such as tunable absorption/emission spectra and conductivity, chemical structure diversity, as well as being environmentally friendly, may facilitate the use of conjugated polymers in many applications, such as in energy storage (fuel cells, batteries, and electrochemical capacitors), photocatalysts for dye removal and water splitting, and in photovoltaics. The major drawbacks of conjugated polymers are their low stability and lower conductivity as compared to metals, which limits their use in transistors and memory devices. Overcoming the current drawbacks in conjugated polymers will increase their potential as candidates for diverse novel applications.

References

1 Hall, N. (2003). Twenty-five years of conducting polymers. *Chem. Commun.* (1): 1–4.

2 Huang, W.-S., Humphrey, B.D., and MacDiarmid, A.G. (1986). Polyaniline, a novel conducting polymer. Morphology and chemistry of its oxidation and reduction in aqueous electrolytes. *J. Chem. Soc., Faraday Trans.* 1 (82): 2385–2400.

3 McCullough, R.D., Lowe, R.D., Jayaraman, M., and Anderson, D.L. (1993). Design, synthesis, and control of conducting polymer architectures: structurally homogeneous poly(3-alkylthiophenes). *J. Org. Chem.* 58: 904–912.

4 Ghosh, S., Remita, H., and Basu, R.N. (2018). Conducting polymers nanostructures as novel materials for efficient solar light harvesting. In: *Visible-Light-Active Photocatalysis: Nanostructured Catalyst Design, Mechanisms, and Applications* (ed. S. Ghosh), 227–252. Weinheim, Germany: Wiley-VCH Verlag GmbH & Co. KGaA.

5 Gangopadhyay, R. and De, A. (2000). Conducting polymer nanocomposites: a brief overview. *Chem. Mater.* 12: 608–622.

6 Tuncel, D. (2019). π-Conjugated nanostructured materials: preparation, properties and photonic applications. *Nanoscale Adv.* 1: 19–33.

7 Shi, Y., Peng, L., Ding, Y. et al. (2015). Nanostructured conductive polymers for advanced energy storage. *Chem. Soc. Rev.* 44: 6684–6696.

8 Gribkova, O.L., Omelchenko, O.D., Tameev, A.R. et al. (2016). The specific effect of graphene additives in polyaniline-based nanocomposite layers on performance characteristics of electroluminescent and photovoltaic devices. *High Energy Chem.* 50: 134–138.

9 Dimitrov, S.D., Schroeder, B.C., Nielsen, C.B. et al. (2016). Singlet exciton lifetimes in conjugated polymer films for organic solar cells. *Polymers* 8: 14.

10 Wang, Q., Jin, Z., Zhang, X. et al. (2017). Cellular architecture-based all-polymer flexible thin-film photodetectors with high performance and stability in harsh environment. *Adv. Mater. Technol.* 2: 1700185.

11 Philip, B., Xie, J., Abraham, J.K., and Varadan, V.K. (2004). A new synthetic route to enhance polyaniline assembly on carbon nanotubes in tubular composites. *Smart Mater. Struct.* 13: N105–N108.

12 Facchetti, A. (2011). Π-conjugated polymers for organic electronics and photovoltaic cell applications. *Chem. Mater.* 23: 733–758.

13 Ghosh, S., Teillout, A.-L., Floresyona, D. et al. (2015). Conducting polymer-supported palladium nanoplates for applications in direct alcohol oxidation. *Int. J. Hydrogen Energy* 40: 4951–4959.

14 Hou, W., Xiao, Y., Han, G., and Lin, J.-Y. (2019). The applications of polymers in solar cells: a review. *Polymers* 11: 143.

15 Bryan, A.M., Santino, L.M., Lu, Y. et al. (2016). Conducting polymers for pseudocapacitive energy storage. *Chem. Mater.* 28: 5989–5998.

16 Muench, S., Wild, A., Friebe, C. et al. (2016). Polymer-based organic batteries. *Chem. Rev.* 116: 9438–9484.

17 Ghosh, S., Remita, H., and Basu, R.N. (2018). Visible-light-induced reduction of Cr(VI) by PDPB-ZnO nanohybrids and its photo-electrochemical response. *Appl. Catal., B* 239: 362–372.

18 Braeken, Y., Cheruku, S., Ethirajan, A., and Maes, W. (2017). Conjugated polymer nanoparticles for bioimaging. *Materials (Basel)* 10: 1420.

19 Stafström, S. and Chao, K.A. (1984). Polaron-bipolaron – soliton doping in polyacetylene. *Phys. Rev. B: Condens. Matter* 30: 2098–2103.

20 Bredas, J.L. and Street, G.B. (1985). Polarons, bipolarons, and solitons in conducting polymers. *Acc. Chem. Res.* 18: 309–315.

21 Ravichandran, R., Sundarrajan, S., Venugopal, J.R. et al. (2010). Applications of conducting polymers and their issues in biomedical engineering. *J. R. Soc. Interface* 7: S559–S579.

22 Wise, D.L., Wnek, G.E., Trantolo, D.J. et al. (1998). *Electrical and Optical Polymer Systems: Fundamentals, Methods and Application*. Boca Raton, FL: CRC Press.

23 Roth, S. and Bleier, H. (1987). Solitons in polyacetylene. *Adv. Phys.* 36: 385–462.

24 Hertel, D., Bässler, H., Scherf, U., and Hörhold, H.H. (1999). Charge carrier transport in conjugated polymers. *J. Chem. Phys.* 110: 9214–9222.

25 Collini, E. and Scholes, G.D. (2009). Coherent intrachain energy migration in a conjugated polymer at room temperature. *Science* 323: 369–373.

26 Le, T.-H., Kim, Y., and Yoon, H. (2017). Electrical and electrochemical properties of conducting polymers. *Polymers* 9: 150.

27 Su, W.P., Schrieffer, J.R., and Heeger, A.J. (1979). Solitons in polyacetylene. *Phys. Rev. Lett.* 42: 1698–1701.

28 MacDiarmid, A.G., Mammone, R.J., Kaner, R.B. et al. (1985). The concept of "doping" of conducting polymers: the role of reduction potentials. *Philos. Trans. R. Soc. London, Ser. A* 314: 3–15.

29 Heeger, A.J., Kivelson, S., Schrieffer, J.R., and Su, W.P. (1988). Solitons in conducting polymers. *Rev. Mod. Phys.* 60: 781–850.

30 Tsukamoto, J. (1992). Recent advances in highly conductive polyacetylene. *Adv. Phys.* 41: 509–546.

31 Tsukamoto, J., Takahashi, A., and Kawasaki, K. (1990). Structure and electrical properties of polyacetylene yielding a conductivity of 10^5 S/cm. *Jpn. J. Appl. Phys.* 29: 125–130.

32 Brédas, J.L., Chance, R.R., and Silbey, R. (1982). Comparative theoretical study of the doping of conjugated polymers: polarons in polyacetylene and polyparaphenylene. *Phys. Rev. B: Condens. Matter* 26: 5843–5854.

33 Chiang, C.K., Fincher, C.R., Park, Y.W. et al. (1977). Electrical conductivity in doped polyacetylene. *Phys. Rev. Lett.* 39: 1098–1101.

34 Furukawa, Y. (1996). Electronic absorption and vibrational spectroscopies of conjugated conducting polymers. *J. Phys. Chem.* 100: 15644–15653.

35 Conwell, E.M. and Mizes, H.A. (1991). Metallic state of polymers with nondegenerate ground states. *Phys. Rev. B: Condens. Matter* 44: 937–942.

36 Zhang, Y., de Boer, B., and Blom, P.W.M. (2009). Controllable molecular doping and charge transport in solution-processed polymer semiconducting layers. *Adv. Funct. Mater.* 19: 1901–1905.

37 Zhang, Y. and Blom, P.W.M. (2011). Electron and hole transport in poly(fluorene-benzothiadiazole). *Appl. Phys. Lett.* 98: 143504.

38 Nollau, A., Pfeiffer, M., Fritz, T., and Leo, K. (2000). Controlled n-type doping of a molecular organic semiconductor: naphthalenetetracarboxylic dianhydride (NTCDA) doped with bis(ethylenedithio)-tetrathiafulvalene (BEDT-TTF). *J. Appl. Phys.* 87: 4340–4343.

39 Patil, A.O., Heeger, A.J., and Wudl, F. (1988). Optical properties of conducting polymers. *Chem. Rev.* 88: 183–200.

40 Abdelhamid, M.E., O'Mullane, A.P., and Snook, G.A. (2015). Storing energy in plastics: a review on conducting polymers & their role in electrochemical energy storage. *RSC Adv.* 5: 11611–11626.

41 Mishra, A.K. (2018). Conducting polymers: concepts and applications. *J. At. Mol. Condens. Nano Phys.* 5: 159–193.

42 Mott, N.F. and Davis, E. (1979). *Electronic Processes in Non-crystalline Materials*. New York, NY: Oxford University Press.

43 Lee, P.A. and Ramakrishnan, T.V. (1985). Disordered electronic systems. *Rev. Mod. Phys.* 57: 287–337.

44 Ahlskog, M. and Menon, R. (1998). The localization-interaction model applied to the direct-current conductivity of metallic conducting polymers. *J. Phys. Condens. Matter* 10: 7171–7181.

45 Anderson, P.W. (1958). Absence of diffusion in certain random lattices. *Phys. Rev.* 109: 1492–1505.

46 Saxena, V., Malhotra, B.D., and Menon, R. (2002). Charge transport and electrical properties of doped conjugated polymers. In: *Handbook of Polymers in Electronics* (ed. B.D. Malhotra), 3–65. Shrewsbury, Shropshire, UK: Rapra Technology Limited.

47 Epstein, A.J., Joo, J., Kohlman, R.S. et al. (1994). Inhomogeneous disorder and the modified Drude metallic state of conducting polymers. *Synth. Met.* 65: 149–157.

48 Kohlman, R.S., Zibold, A., Tanner, D.B. et al. (1997). Limits for metallic conductivity in conducting polymers. *Phys. Rev. Lett.* 78: 3915–3918.

49 Kohlman, R.S., Joo, J., Min, Y.G. et al. (1996). Crossover in electrical frequency response through an insulator–metal transition. *Phys. Rev. Lett.* 77: 2766–2769.

50 Joo, J., Long, S.M., Pouget, J.P. et al. (1998). Charge transport of the mesoscopic metallic state in partially crystalline polyanilines. *Phys. Rev. B: Condens. Matter* 57: 9567–9580.

51 Zuo, F., Angelopoulos, M., MacDiarmid, A.G., and Epstein, A.J. (1987). Transport studies of protonated emeraldine polymer: a granular polymeric metal system. *Phys. Rev. B: Condens. Matter* 36: 3475–3478.

52 Guimard, N.K., Gomez, N., and Schmidt, C.E. (2007). Conducting polymers in biomedical engineering. *Prog. Polym. Sci.* 32: 876–921.

53 Wang, P.-C. and MacDiarmid, A.G. (2008). Vapor phase secondary doping of polyaniline (emeraldine salt) thin films with *o*-chlorophenol investigated by UV–VIS–NIR: effects of primary dopants, substrate surfaces, and pre-treatments of organic vapors. *React. Funct. Polym.* 68: 201–207.

54 Kulszewicz-Bajer, I., Proń, A., Abramowicz, J. et al. (1999). Lewis acid doped polyaniline: preparation and spectroscopic characterization. *Chem. Mater.* 11: 552–556.

55 Chiang, C.K., Blubaugh, E.A., and Yap, W.T. (1984). Electrochemical studies on doping of polyacetylene. *Polymer* 25: 1112–1116.

56 Basescu, N., Liu, Z.X., Moses, D. et al. (1987). High electrical conductivity in doped polyacetylene. *Nature* 327: 403–405.

57 Menon, V.P., Lei, J., and Martin, C.R. (1996). Investigation of molecular and supermolecular structure in template-synthesized polypyrrole tubules and fibrils. *Chem. Mater.* 8: 2382–2390.

58 Zabrodskii, A.G. and Zinov'eva, K.N. (1983). Low-temperature conductivity and metal–insulator transition in compensate n-Ge. *J. Exp. Theor. Phys.* 59: 425.

59 Mott, N.F. (1969). Conduction in non-crystalline materials. *Philos. Mag.* 19: 835–852.

60 Ahlskog, M., Reghu, M., and Heeger, A.J. (1997). The temperature dependence of the conductivity in the critical regime of the metal–insulator transition in conducting polymers. *J. Phys. Condens. Matter* 9: 4145–4156.

61 Ahlskog, M., Reghu, M., Heeger, A.J. et al. (1996). Electronic transport in the metallic state of oriented poly(*p*-phenylenevinylene). *Phys. Rev. B: Condens. Matter* 53: 15529–15537.

62 Chiang, C.K., Park, Y.W., Heeger, A.J. et al. (1978). Conducting polymers: halogen doped polyacetylene. *J. Chem. Phys.* 69: 5098–5104.

63 Roth, S., Bleier, H., and Pukacki, W. (1989). Charge transport in conducting polymers. *Faraday Discuss. Chem. Soc.* 88: 223–233.

64 Roth, S. and Carroll, D. (2004). *One-Dimensional Metals: Conjugated Polymers, Organic Crystals, Carbon Nanotubes*. Weinheim, Germany: Wiley-VCH.

65 Aleshin, A., Kiebooms, R., Menon, R. et al. (1997). Metallic conductivity at low temperatures in poly(3,4-ethylenedioxythiophene) doped with PF_6. *Phys. Rev. B: Condens. Matter* 56: 3659–3663.

66 Lee, K., Cho, S., Heum Park, S. et al. (2006). Metallic transport in polyaniline. *Nature* 441: 65–68.

67 Diaz, A.F., Castillo, J.I., Logan, J.A., and Lee, W.-Y. (1981). Electrochemistry of conducting polypyrrole films. *J. Electroanal. Chem. Interfacial Electrochem.* 129: 115–132.

68 Guay, J., Paynter, R., and Dao, L.H. (1990). Synthesis and characterization of poly(diarylamines): a new class of electrochromic conducting polymers. *Macromolecules* 23: 3598–3605.

69 Bull, R.A., Fan, F.R.F., and Bard, A.J. (1982). Polymer films on electrodes: VII. Electrochemical behavior at polypyrrole-coated platinum and tantalum electrodes. *J. Electrochem. Soc.* 129: 1009–1015.

70 Barsch, U. and Beck, F. (1996). Anodic overoxidation of polythiophenes in wet acetonitrile electrolytes. *Electrochim. Acta* 41: 1761–1771.

71 Novák, P., Rasch, B., and Vielstich, W. (1991). Overoxidation of polypyrrole in propylene carbonate: an in situ FTIR study. *J. Electrochem. Soc.* 138: 3300–3304.

72 Lewis, T.W., Wallace, G.G., Kim, C.Y., and Kim, D.Y. (1997). Studies of the overoxidation of polypyrrole. *Synth. Met.* 84: 403–404.

73 Li, Y. and Qian, R. (2000). Electrochemical overoxidation of conducting polypyrrole nitrate film in aqueous solutions. *Electrochim. Acta* 45: 1727–1731.

74 Pei, Q. and Inganaes, O. (1992). Electrochemical applications of the bending beam method. 1. Mass transport and volume changes in polypyrrole during redox. *J. Phys. Chem.* 96: 10507–10514.

75 Lizarraga, L., Marı́ a Andrade, E., and Victor Molina, F. (2004). Swelling and volume changes of polyaniline upon redox switching. *J. Electroanal. Chem.* 561: 127–135.

76 Otero, T.F., Angulo, E., Rodríguez, J., and Santamaría, C. (1992). Electrochemomechanical properties from a bilayer: polypyrrole/non-conducting and flexible material – artificial muscle. *J. Electroanal. Chem.* 341: 369–375.

77 Kertész, M., Vonderviszt, F., and Pekker, S. (1982). Change of geometry of polyacetylene upon charge transfer. *Chem. Phys. Lett.* 90: 430–433.

78 Bay, L., Jacobsen, T., Skaarup, S., and West, K. (2001). Mechanism of actuation in conducting polymers: osmotic expansion. *J. Phys. Chem. B* 105: 8492–8497.

79 Kilmartin, P.A. and Travas-Sejdic, J. (2010). Nanostructural aspects of conducting-polymer actuators. In: *Nanostructured Conductive Polymers*, 599–630. New York, NY: Wiley.

80 Takashima, W., Pandey, S.S., Fuchiwaki, M., and Kaneto, K. (2002). Cyclic step-voltammetric analysis of cation-driven and anion-driven actuation in polypyrrole films. *Jpn. J. Appl. Phys.* 41: 7532–7536.

81 Naoi, K., Lien, M., and Smyrl, W.H. (1991). Quartz crystal microbalance study: ionic motion across conducting polymers. *J. Electrochem. Soc.* 138: 440–445.

82 Qiu, Y.-J. and Reynolds, J.R. (1991). Dopant anion controlled ion transport behavior of polypyrrole. *Polym. Eng. Sci.* 31: 417–421.

83 Matencio, T., De Paoli, M.A., Peres, R.C.D. et al. (1995). Ionic exchanges in dodecylbenzenesulfonate doped polypyrrole Part 1. Optical beam deflection studies. *Synth. Met.* 72: 59–64.

84 Maw, S., Smela, E., Yoshida, K., and Stein, R.B. (2005). Effects of monomer and electrolyte concentrations on actuation of PPy(DBS) bilayers. *Synth. Met.* 155: 18–26.

85 Aydemir, N., Kilmartin, P.A., Travas-Sejdic, J. et al. (2015). Electrolyte and solvent effects in PPy/DBS linear actuators. *Sens. Actuators, B* 216: 24–32.

86 Barnes, A., Despotakis, A., Wong, T.C.P. et al. (1998). Towards a 'smart window' for microwave applications. *Smart Mater. Struct.* 7: 752–758.

87 Pagès, H., Topart, P., and Lemordant, D. (2001). Wide band electrochromic displays based on thin conducting polymer films. *Electrochim. Acta* 46: 2137–2143.

88 Ji, L., Dai, Y., Yan, S. et al. (2016). A fast electrochromic polymer based on TEMPO substituted polytriphenylamine. *Sci. Rep.* 6: 30068.

89 Schwendeman, I., Hwang, J., Welsh, D.M. et al. (2001). Combined visible and infrared electrochromism using dual polymer devices. *Adv. Mater.* 13: 634–637.

90 Barford, W. (2013). Excitons in conjugated polymers: a tale of two particles. *J. Phys. Chem. A* 117: 2665–2671.

91 Scholes, G.D. and Rumbles, G. (2006). Excitons in nanoscale systems. *Nat. Mater.* 5: 683–696.

92 Cornil, J., Beljonne, D., Calbert, J.-P., and Brédas, J.-L. (2001). Interchain interactions in organic π-conjugated materials: impact on electronic structure, optical response, and charge transport. *Adv. Mater.* 13: 1053–1067.

93 Salzner, U., Lagowski, J.B., Pickup, P.G., and Poirier, R.A. (1998). Comparison of geometries and electronic structures of polyacetylene, polyborole, polycyclopentadiene, polypyrrole, polyfuran, polysilole, polyphosphole, polythiophene, polyselenophene and polytellurophene. *Synth. Met.* 96: 177–189.

94 Jenekhe, S.A. (1987). New electronically conducting polymers: effects of molecular structure on intrinsic electronic properties. In: *Conducting Polymers* (ed. L. Alcácer), 149. Dordrecht: Springer Netherlands.

95 Roncali, J. (2007). Molecular engineering of the band gap of π-conjugated systems: facing technological applications. *Macromol. Rapid Commun.* 28: 1761–1775.

96 Cade, P.E. (1967). The electron affinities of the diatomic hydrides CH, NH, SiH and PH. *Proc. Phys. Soc.* 91: 842–854.

97 Matsumoto, T., Tanaka, K., and Chujo, Y. (2015). Synthesis and characterization of gallafluorene-containing conjugated polymers: control of emission colors and electronic effects of gallafluorene units on π-conjugation system. *Macromolecules* 48: 1343–1351.

98 Burroughes, J.H., Bradley, D.D.C., Brown, A.R. et al. (1990). Light-emitting diodes based on conjugated polymers. *Nature* 347: 539–541.

99 Ariu, M., Lidzey, D.G., Sims, M. et al. (2002). The effect of morphology on the temperature-dependent photoluminescence quantum efficiency of the conjugated polymer poly(9,9-dioctylfluorene). *J. Phys. Condens. Matter* 14: 9975–9986.

100 Asada, K., Kobayashi, T., and Naito, H. (2006). Control of effective conjugation length in polyfluorene thin films. *Jpn. J. Appl. Phys.* 45: L247–L249.

101 Greenham, N.C., Samuel, I.D.W., Hayes, G.R. et al. (1995). Measurement of absolute photoluminescence quantum efficiencies in conjugated polymers. *Chem. Phys. Lett.* 241: 89–96.

102 Piris, J., Dykstra, T.E., Bakulin, A.A. et al. (2009). Photogeneration and ultrafast dynamics of excitons and charges in P3HT/PCBM blends. *J. Phys. Chem. C* 113: 14500–14506.

103 Hou, L., Adhikari, S., Tian, Y. et al. (2017). Absorption and quantum yield of single conjugated polymer poly[2-methoxy-5-(2-ethylhexyloxy)-1,4-phenylenevinylene] (MEH-PPV) molecules. *Nano Lett.* 17: 1575–1581.

104 Sun, K., Chen, H., Wang, L. et al. (2014). Size-dependent property and cell labeling of semiconducting polymer dots. *ACS Appl. Mater. Interfaces* 6: 10802–10812.

105 Schütze, F., Krumova, M., and Mecking, S. (2015). Size control of spherical and anisotropic fluorescent polymer nanoparticles via precise rigid molecules. *Macromolecules* 48: 3900–3906.

106 Botiz, I., Astilean, S., and Stingelin, N. (2016). Altering the emission properties of conjugated polymers. *Polym. Int.* 65: 157–163.

107 Schneider, J.A., Dadvand, A., Wen, W., and Perepichka, D.F. (2013). Tuning the electronic properties of poly(thienothiophene vinylene)s via alkylsulfanyl and alkylsulfonyl substituents. *Macromolecules* 46: 9231–9239.

108 Ramsdale, C.M., Barker, J.A., Arias, A.C. et al. (2002). The origin of the open-circuit voltage in polyfluorene-based photovoltaic devices. *J. Appl. Phys.* 92: 4266–4270.

109 Kietzke, T., Neher, D., Kumke, M. et al. (2004). A nanoparticle approach to control the phase separation in polyfluorene photovoltaic devices. *Macromolecules* 37: 4882–4890.

110 Beljonne, D., Pourtois, G., Silva, C. et al. (2002). Interchain vs. intrachain energy transfer in acceptor-capped conjugated polymers. *Proc. Natl. Acad. Sci. U.S.A.* 99: 10982–10987.

111 Yu, J., Hu, D., and Barbara, P.F. (2000). Unmasking electronic energy transfer of conjugated polymers by suppression of O_2 quenching. *Science* 289: 1327–1330.

112 Laquai, F., Park, Y.-S., Kim, J.-J., and Basché, T. (2009). Excitation energy transfer in organic materials: from fundamentals to optoelectronic devices. *Macromol. Rapid Commun.* 30: 1203–1231.

113 Yersin, H. (2004). Triplet emitters for OLED applications. Mechanisms of exciton trapping and control of emission properties. In: *Transition Metal and Rare Earth Compounds: Excited States, Transitions, Interactions III* (ed. H. Yersin), 1–26. Berlin, Heidelberg: Springer Berlin Heidelberg.

114 Zhang, Y., Wang, Y., Song, J. et al. (2018). Near-infrared emitting materials via harvesting triplet excitons: molecular design, properties, and application in organic light emitting diodes. *Adv. Opt. Mater.* 6: 1800466.

115 Chen, R., Tang, Y., Wan, Y. et al. (2017). Promoting singlet/triplet exciton transformation in organic optoelectronic molecules: role of excited state transition configuration. *Sci. Rep.* 7: 6225.

116 Li, D., Hu, Y., and Liao, L.-S. (2019). Triplet exciton harvesting by multi-process energy transfer in fluorescent organic light-emitting diodes. *J. Mater. Chem. C* 7: 977–985.

117 Tao, Y., Yuan, K., Chen, T. et al. (2014). Thermally activated delayed fluorescence materials towards the breakthrough of organoelectronics. *Adv. Mater.* 26: 7931–7958.

118 Tritsch, J.R., Chan, W.-L., Wu, X. et al. (2013). Harvesting singlet fission for solar energy conversion via triplet energy transfer. *Nat. Commun.* 4: 2679.

119 Pope, M. and Swenberg, C.E. (1999). *Electronic Processes in Organic Crystals and Polymers*, 2e. United Kingdom: Oxford University Press.

120 Lin, J.D.A., Mikhnenko, O.V., Chen, J. et al. (2014). Systematic study of exciton diffusion length in organic semiconductors by six experimental methods. *Mater. Horiz.* 1: 280–285.

121 Tamai, Y., Ohkita, H., Benten, H., and Ito, S. (2015). Exciton diffusion in conjugated polymers: from fundamental understanding to improvement in photovoltaic conversion efficiency. *J. Phys. Chem. Lett.* 6: 3417–3428.

122 Hedley, G.J., Ruseckas, A., and Samuel, I.D.W. (2017). Light harvesting for organic photovoltaics. *Chem. Rev.* 117: 796–837.

123 Antoniadis, H., Rothberg, L.J., Papadimitrakopoulos, F. et al. (1994). Enhanced carrier photogeneration by defects in conjugated polymers and its mechanism. *Phys. Rev. B: Condens. Matter* 50: 14911–14915.

124 Burin, A.L. and Ratner, M.A. (2000). Exciton migration and cathode quenching in organic light emitting diodes. *J. Phys. Chem. A* 104: 4704–4710.

125 Park, H.-W., Kim, T., Huh, J. et al. (2012). Anisotropic growth control of polyaniline nanostructures and their morphology-dependent electrochemical characteristics. *ACS Nano.* 6: 7624–7633.

126 Laviron, E. (1979). General expression of the linear potential sweep voltammogram in the case of diffusionless electrochemical systems. *J. Electroanal. Chem. Interfacial Electrochem.* 101: 19–28.